

BOLU ABANT IZZET BAYSAL UNIVERSITY
THE GRADUATE SCHOOL OF NATURAL AND APPLIED
SCIENCES



INVESTIGATION OF TRANSPORT PROPERTIES OF
SUPERCONDUCTING MgB₂/Fe WIRES FABRICATED BY MAGNESIUM
COATING METHOD

MASTER OF SCIENCE

DOĞAN AVCI

BOLU, SEPTEMBER 2019

BOLU ABANT IZZET BAYSAL UNIVERSITY
THE GRADUATE SCHOOL OF NATURAL AND APPLIED
SCIENCES
DEPARTMENT OF PHYSICS



INVESTIGATION OF TRANSPORT PROPERTIES OF
SUPERCONDUCTING MgB_2/Fe WIRES FABRICATED BY MAGNESIUM
COATING METHOD

MASTER OF SCIENCE

DOĞAN AVCI

BOLU, SEPTEMBER 2019


APPROVAL OF THE THESIS

INVESTIGATION OF TRANSPORT PROPERTIES OF SUPERCONDUCTING MgB₂/Fe WIRES FABRICATED BY MAGNESIUM COATING METHOD submitted by Doğan AVCI in partial fulfillment of the requirements for the degree of Master of Science in Department of Physics, The Graduate School of Natural and Applied Sciences of BOLU ABANT İZZET BAYSAL UNIVERSITY in 09/09/2019 by

Examining Committee Members

Signature

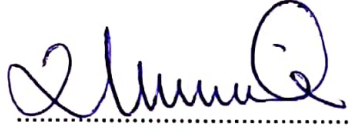
Supervisor
PROF. DR. HAKAN YETİŞ
Bolu Abant İzzet Baysal University


.....

Member
PROF. DR. İBRAHİM BELENLİ
Bolu Abant İzzet Baysal University


.....

Member
PROF. DR. ÖZGÜR ÖZTÜRK
Kastamonu University

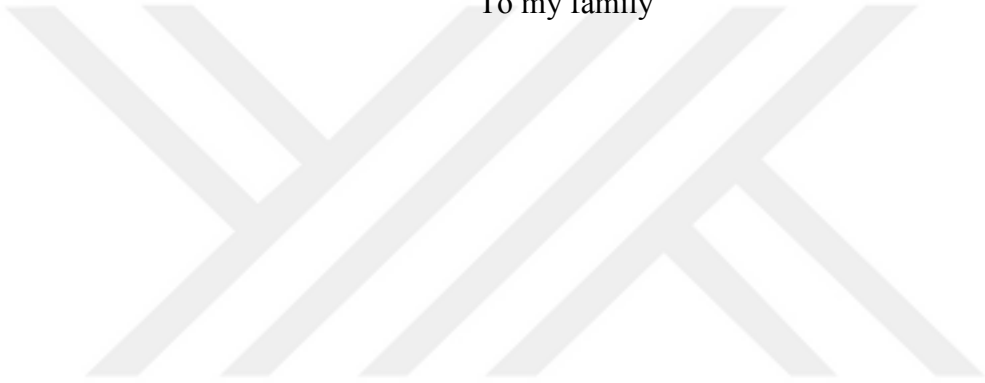

.....

Prof. Dr. Ömer ÖZYURT


.....

Director of Graduate School of Natural and Applied Sciences ✓

To my family



DECLARATION

I hereby declare that all information in this document has been obtained and presented in accordance with academic rules and ethical conduct. I also declare that, as required by these rules and conduct, I have fully cited and referenced all material and results that are not original to this work.

Dođan AVCI



ABSTRACT

INVESTIGATION OF TRANSPORT PROPERTIES OF SUPERCONDUCTING MgB_2/Fe WIRES FABRICATED BY MAGNESIUM COATING METHOD

MSC THESIS
DOĞAN AVCI

BOLU ABANT IZZET BAYSAL UNIVERSITY GRADUATE SCHOOL OF
NATURAL AND APPLIED SCIENCES

DEPARTMENT OF PHYSICS
(SUPERVISOR: PROF. DR. HAKAN YETİŞ)

BOLU, SEPTEMBER 2019

In this thesis, an experimental study which shows the effect of excess magnesium addition by evaporation technique on the current carrying properties of a single-core *in-situ* MgB_2/Fe superconducting wire is presented. The initial excess magnesium was introduced by using a special evaporation technique in which a small amount of excess magnesium with <1wt. % was first coated by means of evaporation method into an empty iron tube, and then stoichiometric $Mg + 2B$ precursor powder was packed into this Mg coated tube in powder or pellet forms. In order to make a comparison, the excess Mg was also introduced by a mixing method into the stoichiometric $Mg + 2B$ powder in which the final mixture was packed into an empty iron tube by pellet-in-tube method again. The latter non-stoichiometric wires were prepared to contain different amount of excess magnesium with ratios 1wt. % and 5wt. % of the total $Mg + 2B$ mixture weight. The reasons for the use of Mg-coating method are to ensure a uniform distribution of small amount of excess Mg along the wire and to reduce the formation of Fe_2B in the core/sheath interface region. Transport measurements were carried out in order to determine the critical temperature, the engineering critical current density, the n -value, the resistivity and connectivity of the stoichiometric and non-stoichiometric wires produced by a cold wire drawing. The results revealed that the excess Mg significantly enhances the structural, superconducting, and transport properties of the MgB_2/Fe wire. The most important result is that the Mg-coated sample has the best transport properties under the magnetic field. The highest J_{ce} and n -values were obtained for the Mg-coated wire with the lowest starting excess Mg ratio between the non-stoichiometric wires. Discussions in this thesis are expected to make a contribution to the debates on Mg stoichiometry which influences the critical current density of MgB_2 wires under the external magnetic field.

KEYWORDS: Superconductivity, MgB_2 , Excess magnesium, Mg Coating, MgB_2 wire.

ÖZET

MAGNEZYUM KAPLAMA YÖNTEMİ İLE ÜRETİLEN MgB_2/Fe SÜPERİLETKEN TELLERİN TRANSPORT ÖZELLİKLERİNİN

ARAŞTIRILMASI
YÜKSEK LİSANS TEZİ
DOĞAN AVCI

BOLU ABANT İZZET BAYSAL ÜNİVERSİTESİ
FEN BİLİMLERİ ENSTİTÜSÜ

FİZİK ANABİLİM DALI
(TEZ DANIŞMANI: PROF. DR. HAKAN YETİŞ)

BOLU, EYLÜL - 2019

Bu tez çalışmasında, fazlalık magnezyumun buharlaştırma tekniği ile ilave edilmesinin tek damarlı *in-situ* MgB_2/Fe süperiletken bir telin akım taşıma özellikleri üzerindeki etkisini gösteren deneysel bir çalışma sunulmuştur. İlk olarak düşük miktarda fazlalık Mg (ağırlıkça $< \%1$) özel bir buharlaştırma yöntemi ile boş bir demir borunun iç yüzeyine kaplandı ve daha sonra bu Mg kaplı boru içerisine stokiyometrik $Mg + 2B$ öncü tozu tablet veya toz formunda doldurularak tel üretimi gerçekleştirildi. Karşılaştırma yapabilmek için fazla magnezyumun doğrudan karışım yöntemi kullanılarak dâhil edildiği teller de üretildi. Toplam $Mg + 2B$ karışımının ağırlıkça $\% 1$ ve $\% 5$ 'i oranlarında fazladan magnezyum içerecek şekilde hazırlanan bu tellerde, fazlalık Mg stokiyometrik $Mg + 2B$ tozuna karıştırma yöntemiyle ilave edildi ve elde edilen son karışım tüp içinde tablet yöntemi ile boş bir demir boru içerisine dolduruldu. Mg-kaplama yöntemi kullanımının nedenleri; tel boyunca az miktarda fazlalık magnezyumun düzgün bir şekilde dağılımını sağlamak ve çekirdek/kılıf ara yüzey bölgesinde Fe_2B faz oluşumunu azaltmaktır. Soğuk tel çekme yöntemi ile üretilen stokiyometrik ve stokiyometrik olmayan tellerin kritik sıcaklığını, mühendislik kritik akım yoğunluğunu, n -değerini, öz direncini ve tanecikler arası bağlantılarını belirlemek için akım taşıma ölçümleri yapılmıştır. Sonuçlar, fazlalık magnezyumun MgB_2/Fe telinin yapısal, süperiletken ve akım taşıma özelliklerini önemli ölçüde arttırdığını ortaya koymuştur. En önemli sonuç, Mg kaplı numunenin manyetik alan altında en iyi akım taşıma özelliklerine sahip olmasıdır. En yüksek J_{ce} ve n değerleri, stokiyometrik olmayan teller arasında en düşük başlangıç fazlalık Mg oranına sahip Mg kaplı tel için elde edildi. Bu tez çalışmasının, dış manyetik alan altında MgB_2 tellerinin kritik akım yoğunluğunu etkileyen Mg stokiyometrisi hakkındaki güncel tartışmalara katkı yapması beklenmektedir.

ANAHTAR KELİMELER: Süperiletkenlik, MgB_2 , Fazlalık magnezyum, Mg Kaplama, MgB_2 tel.

TABLE OF CONTENTS

	<u>Page</u>
ABSTRACT	v
ÖZET.....	vi
TABLE OF CONTENTS.....	vii
LIST OF FIGURES	ix
LIST OF TABLES	xii
LIST OF ABBREVIATIONS ANDSYMBOLS	xiii
1. INTRODUCTION	1
2. AIM AND SCOPE OF THE STUDY	5
3. SUPERCONDUCTIVITY	6
3.1 Discovery of Superconductivity and Superconductors	6
3.2 Zero Electrical Resistivity and Perfect Diamagnetism.....	8
3.3 Meissner Effect.....	9
3.4 Magnetic Properties of Superconductors	10
3.4.1 Type I Superconductors	10
3.4.2 Type II Superconductors.....	11
3.5 Critical Parameters of Superconductors	12
3.5.1 Critical Temperature (T_c).....	13
3.5.2 Critical Magnetic Field (B_c).....	14
3.5.3 Critical Current Density (J_c).....	14
3.6 London Theory	15
3.6.1 London Penetration Depth	16
3.7 Ginzburg Landau Theory	17
3.7.1 Ginzburg-Landau Parameter	17
3.8 BCS Theory	18
4. MAGNESIUM DIBORIDE SUPERCONDUCTOR.....	20
4.1 Discovery of MgB_2	20
4.2 Crystal Structure of MgB_2	20
4.3 Electronic Structure of MgB_2	21
4.4 Superconducting Mechanism in MgB_2	22
4.5 Anisotropy (γ)	22
4.6 Isotope Effect	23
4.7 Grain Connectivity, Porosity and Weak-Link	24
5. MgB_2 WIRE AND ITS DEVELOPMENT	26
5.1 Fabrication Techniques	26
5.1.1 PIT and CTFE Methods	26
5.1.2 IMD Method	26
5.1.3 HIP and CHPD Methods.....	27
5.1.4 PeIT Method	28
5.2 Mechanical Properties	28

5.3	Transport Characterization Techniques.....	29
5.3.1	Resistivity and Connectivity Analysis.....	29
5.3.2	Transport J_c and Flux Pinning Mechanism.....	30
5.4	Applications of MgB ₂ Wires.....	30
6.	EXPERIMENTAL SETUP	32
6.1	Internal Magnesium Coating Method.....	32
6.2	Preparation of <i>in-situ</i> Mg+2B Powder.....	33
6.3	Production of <i>in-situ</i> MgB ₂ /Fe Mono and Multi-filament Wires.....	35
6.4	Heat Treatments.....	36
6.5	The Structural Analysis Method.....	37
6.6	Surface Analysis.....	38
6.7	Electrical Characterization Techniques.....	39
7.	RESULTS AND DISCUSSIONS	41
7.1	Temperature Dependent Resistivity Measurements.....	41
7.2	Current-Voltage Measurements.....	51
7.3	XRD Measurements.....	58
7.4	Scanning Electron Microscope (SEM) Analysis.....	62
8.	CONCLUSIONS.....	71
9.	REFERENCES	73
10.	CURRICULUM VITAE.....	81

LIST OF FIGURES

	<u>Page</u>
Figure 3.1. The graph represents the measurement of resistance versus temperature of a mercury rod.	6
Figure 3.2. Discovery of superconducting materials with their critical temperatures (T_c).....	7
Figure 3.3. Schematic representation of Meissner effect for a superconductor under zero field-cooled and field-cooled conditions.	9
Figure 3.4. Temperature dependence of B_c for a type I superconductor. Except for Nb, pure samples of all superconducting elements exhibit type I behavior.	11
Figure 3.5. The magnetization curves of type I and type II superconductors. The phase regions are represented as I: Meissner state, II: Mixed state, and III: Normal state. The superconductivity is completely lost in the normal state.....	12
Figure 3.6. Temperature dependence of electrical resistivity of metal and a superconductor. T_c is the critical temperature of a superconductor and ρ_o is the residual resistivity of a metal at 0K. A second order phase transition from normal state to superconducting state is observed below the T_c	13
Figure 3.7. The electron-phonon interaction. The electron 1 and electron 2 form a Cooper pair.	188
Figure 4.1. The crystal structure of Magnesium diboride superconductor (Akimitsu et al., 2001)	20
Figure 4.2. Porous microstructure in an <i>in-situ</i> MgB ₂ superconducting wire (SEM analysis).....	25
Figure 5.1. <i>In-situ</i> pellet-in-tube (PeIT) method for MgB ₂ /Fe wire fabrication ..	28
Figure 6.1. A vertical furnace and experimental set up for magnesium coating process.	32
Figure 6.2. Ball milling machine which is used to obtain homogeneous mixture of stoichiometric and non-stoichiometric Mg+2B powders.	33
Figure 6.3. Mg+2B pellets and production units of hydraulic press and die.	34
Figure 6.4. PIT or PeIT processed, sealed iron tube which is suitable for wire drawing.....	34
Figure 6.5. Dies with different internal diameters, two groove rolling machines and long wire drawing machine that are used for the production of wires.	35
Figure 6.6. A programmable tube furnace with required installation parts.	36
Figure 6.7. X-ray diffractometer for crystal structure analysis.	38
Figure 6.8. Scanning electron microscope device (JEOL 6390-LV).	39
Figure 6.9. A polishing machine is on the left and the mounting press is on the right.....	39
Figure 6.10. Electrical characterization measurement system.	40
Figure 7.1. Temperature dependent resistivity ($\rho - T$) curves of (a) Mg-coated and (b) normal mono core MgB ₂ /Fe superconducting wires with OD =	

	0.81mm as functions of sintering time and temperatures. (A: 700°C-1h, B: 700°C-2h, C: 750°C-1h, D: 750°C-2h).....	42
Figure 7.2.	(a) The offset critical temperature ($T_{c,offset}$) and (b) superconducting phase transition width ($\Delta T = T_{c,offset} - T_{c,onset}$) values of Mg-coated and normal wires. The samples are coded as 1- 700°C, 1h, 2- 700°C, 2h, 3- 750°C, 1h, and 4- 750°C, 2h according to heat treatment time and temperature. The inset in Figure 7.2(a) represent the $T_{c,onset}$ values for the same samples.....	43
Figure 7.3.	The resistivity versus temperature curves for (a) Mg-coated, (b) 1wt. % excess-Mg, and (c) 5wt. % excess-Mg mono core MgB ₂ /Fe wires with 0.81mm outer diameter(on the next page). The same heat treatment conditions were applied for all samples. Mg-coated wire has an excess-Mg which is less than 1wt. % of total Mg+2B. All the samples were produced by using the PeIT method. (A: 700°C-1h, B: 700°C-2h, C: 750°C-1h, D: 750°C-2h).....	45-46
Figure 7.4.	(a) $T_{c,offset}$, (b) $T_{c,onset}$, and (c) ΔT values for Mg-coated, 1wt. %, and 5wt. % excess-Mg wires produced by PeIT method. The data is extracted from the ρ - T curves in Figure 7.3.....	47
Figure 7.5.	The temperature dependent resistivity curves of Mg-coated (L) and normal (K) multifilamentary in-situ PIT processed MgB ₂ /Fe wires sintered at 700°C for 1h. The number of filaments in these wires is 18+1.	48
Figure 7.6.	Temperature dependent resistivity values of MgB ₂ /Fe wire samples heat treated at 700°C for 1h. The sample codes: 1A- Normal, 3A- Mg-coated, 5A- 1wt. % excess-Mg and 6A- 5wt. % excess-Mg. The inset shows $\rho(T)$ characteristics of the same wires annealed at 750°C 1h.....	49
Figure 7.7.	The E vs. J_e curves obtained for (a) Mg-coated and (b) normal superconducting wires at various sintering time and temperatures. The total wire diameter is 0.81mm and both samples were produced by using PIT method.....	52
Figure 7.8.	E vs. J_e characteristics for (a) 1wt. % excess-Mg, (b) 5wt. % excess-Mg, and (c) less than 1wt. % Mg-coated wire samples, respectively. All samples were fabricated by using the PeIT method.	54
Figure 7.9.	$J_{ce} - B$ curves at $T = 28K$ obtained for all sample groups. The engineering critical current density values were determined according to $1\mu V/cm$ criteria.	55
Figure 7.10.	The n -values calculated for normal, Mg-coated, and excess-Mg (1wt. % and 5wt. %) MgB ₂ superconducting wire samples.....	56
Figure 7.11.	$J_{ce} - B$ curves of four PIT processed Mg-coated MgB ₂ /Fe wire samples measured in liquid helium environment.	57
Figure 7.12.	E vs. J_e curves of Mg-coated and normal in-situ MgB ₂ /Fe multifilamentary wires.	58
Figure 7.13.	XRD patterns of (a) normal and (b) Mg-coated wires produced by using PIT initial filling method.....	60
Figure 7.14.	XRD patterns of all samples that are heat treated at (a) 700°C and (b) 750°C for 1h, respectively.	61-62
Figure 7.15.	This image shows the elemental map analysis of a piece from Mg-coated Fe tube. Different colors represent the elements as follows: Red (carbon), green (oxygen), blue (magnesium), and pink (iron). .63	

Figure 7.16. This figure shows the cross sections of normal and Mg-coated samples. (a) and (c) Mg-coated samples synthesized at temperatures of 700°C and 750°C for 2h, respectively. (b) and (d) Normal samples synthesized at $T = 700^{\circ}\text{C}$ and 750°C for 2h, respectively. These samples were produced by using PIT method.	64
Figure 7.17. SEM images of PIT normal samples are seen on the right (b, d, f, h) and PIT Mg-coated samples are seen on the left (a, c, e, g). Top 2 rows are at x5000 magnification and bottom 2 rows are at x10000 magnification. Micrographs in the first and third rows were taken from the wires synthesized at 700°C and others were taken from the wires synthesized at 750°C, for 2h.	65
Figure 7.18. Microstructures of PeIT processed (a) normal (stoichiometric) MgB_2 wire synthesized at 750°C for 1h, (b) < 1wt. % Mg-coated wire synthesized at 700°C for 1h, and (c) 5wt. % excess-Mg wire synthesized at 700°C for 1h. These images obtained from the lateral surface of stripped wires with magnification of 20000×.	66
Figure 7.19. Spot EDS analysis of Mg-coated wire taken from different surface regions.	67
Figure 7.20. EDS analysis results for <1wt. % Mg-coated wire synthesized at 700°C for 1h. The locations of spots 1 (a) and 6 (b, on the next page) are shown in Figure 7.19.	67-68
Figure 7.21. Micrographs for (a-b) the normal (stoichiometric) sample synthesized at 750°C for 1h, (c-d) <1wt. % Mg-coated sample synthesized at 700°C for 1h, and (e-f) 5wt. % excess-Mg sample synthesized at 700°C for 1h. Magnifications are 20000× at left column and 5000× at right column. These samples were produced by using PeIT method.	69

LIST OF TABLES

	<u>Page</u>
Table 4.1. The isotope effect coefficient values for some elements (Mourachkine, 2004)	24
Table 6.1. Table represents all samples in groups.....	37
Table 7.1. $T_{c,offset}$, $T_{c,onset}$, and ΔT values for normal (K) and Mg-coated (L) MgB ₂ /Fe multi-filamentary wires.....	49
Table 7.2. The RRR and A_F values of the MgB ₂ /Fe wire samples heat treated at 700 and 750°C for 1h. $\Delta\rho_{ideal} = 7.3 \mu\Omega.cm$ (Chen et al., 2008). MgB ₂ core diameters are 0.56mm for Mg-coated - normal wire samples and 0.58mm for 1wt. % - 5wt. % excess-Mg samples.....	51

LIST OF ABBREVIATIONS AND SYMBOLS

PIT	: Powder In Tube
PeIT	: Pellet In Tube
HIP	: Hot Isostatic Pressure
IMD	: Internal Magnesium Diffusion
LIMD	: Localized Internal Magnesium Diffusion
CHPD	: Cold High Pressure Densification
CTFF	: Continuous Tube Filling and Forming
MRI	: Magnetic Resonance Imaging
FCL	: Fault Current Limiter
SMES	: Superconducting Magnetic Energy Storage
LTSs	: Low Temperature Superconductors
HTSCs	: High Temperature Superconductors
ZFC	: Zero Field Cooling
NS	: Normal-Superconductor
GL	: Ginzburg-Landau
BCS	: Bardeen-Cooper-Schrieffer
DOS	: Density of state
EDS	: Electron Dispersive X-ray Spectroscopy
SEM	: Scanning Electron Microscope
XRD	: X-ray Diffraction
PVZ	: Pavezyum
RRR	: Residual Resistance Ratio
OD	: Outer diameter
ID	: Inner diameter
SS	: Stainless-Steel
2D	: Two-dimension
J_c	: Critical current density
J_{ce}	: Engineering critical current density
T_c	: Critical temperature
B_{c1}	: Lower critical field
B_{c2}	: Upper critical field
B_{irr}	: Irreversibility field

I_c	: Critical current
μ_0	: Permeability of free space
α	: Isotope effect coefficient
Φ	: Flux
κ	: Ginzburg-Landau parameter
ξ	: Coherence length
λ	: Penetration depth
ψ	: Wave function
h	: Planck constant
M	: Magnetization
χ	: Magnetic susceptibility
e	: Electron charge
G	: Gibbs free energy
F_p	: Pinning force
n	: Electron density
γ	: Anisotropy factor
A_f	: Active cross-sectional Area
ρ	: Resistivity
V	: Voltage
R	: Resistance
DC	: Direct Current
AC	: Alternative Current
T	: Temperature
I	: Current
K	: Kelvin
°C	: Degrees Celsius
A	: Ampere
T	: Tesla
cm	: Centimeter
Θ	: Bragg-angle
E_f	: Fermi Energy
μ	: Micro
mm	: Milimeter
Ω	: Ohm

 	: Parallel
LHe	: Liquid-Helium
LH2	: Liquid-Hydrogen
h	: Hour
GPa	: Giga Pascal
MPa	: Mega Pascal



ACKNOWLEDGEMENTS

I would like to thank my supervisor Prof. Dr. Hakan Yetiř for his advices and guidance throughout the research. He has always encouraged me to pursue innovative approaches during the experimental studies. He helped me greatly in the process of formation of the thesis.

I would also like to thank Prof. Dr. İbrahim Belenli and Prof. Dr. Ali Gençer for their suggestions, comments and support during the thesis process.

I am grateful to Assoc. Prof. Dr. Mustafa Akdođan and Prof. Dr. Özgür Öztürk due to their contribution to the acquisition of SEM measurements.

I am also grateful to Assist. Prof. Dr. Fırat Karabođa for his contributions and suggestions to my thesis. He always helped me through the experimental study for my thesis. He supported me in all the experimental processes in my thesis.

I especially thank my family for their patience, love, motivation and support during my thesis study. I also thank my sweetheart Nisan Erkuř for her motivation, support and advices. I am grateful to my close friends Umut Keskin, Kaan Yüksel Oyulmaz, Özgün Karadeniz, Sinan Öztel and Ufuk Üstün for their help, support and advice during the thesis period.

This study was supported by the Bolu Abant İzzet Baysal University, Department of Scientific Research Projects under the contract 2017.03.02.1126 and the Scientific and Technological Research Council of Turkey, Grant No: 217M665.

1. INTRODUCTION

There have been numerous efforts in order to improve the critical parameters of MgB₂ wire such as critical current density (J_c), upper critical field (B_{c2}), and irreversibility field (B_{irr}) in terms of its usage in superconducting applications (Flükiger, 2016). MgB₂ wires can be produced via *ex-situ* or *in-situ* techniques, but the *in-situ* process is considered to be more effective in improving the wire properties. The main disadvantage of *in-situ* processed MgB₂ wire is that it has a highly porous core structure which reduces the critical current density (Collings et al., 2008). Main source of the porosity is due to the volume contraction resulting from the chemical reaction of magnesium with boron during the reaction process (Yamamoto et al., 2007). This intrinsic problem encountered in the production of *in-situ* wire is a matter that needs to be solved in order to improve the current carrying properties of the MgB₂ wires. Some progressive ideas have been developed upon the densification of the MgB₂ wire core while the chemical reaction is taking place (Serquis et al., 2008; Gajda et al., 2013). A hot isostatic pressure (HIP) method in which an *in-situ* processed Mg+2B wire is heat treated under hot isostatic gas pressure seems completely handle the porosity problem. However, the HIP method can only be applied on a small part of the wire and adversely affects the wire roundness due to the application of high pressure in a solid state media (Cetner et al., 2015). When the HIP method is applied to multi-filamentary wires, it may cause some structural problems depending on the strand geometry and sheath material (Cetner et al., 2012). Another special technique called the reactive liquid magnesium infiltration was developed by Giunchi et al. and it is a modified version of the PIT method (Giunchi et al., 2003). In this method, a Mg rod is placed to the centre of the niobium/steel composite tube and boron powder is filled around the Mg rod. The wires produced by this method were found to be very compact, fine grains and dense MgB₂ layer at core/sheath interface region. Hur et al. improved the infiltration method and fabricated an MgB₂ wire with a J_c ($T = 4.2\text{K}$, $B = 8\text{T}$) of more than 10^5A/cm^2 by internal magnesium diffusion (IMD) method with the support of nano SiC addition at low annealing temperatures (Hur et al., 2008). The IMD wire has a high critical current density but the centre of the wire remains empty due to the diffusion of magnesium rod towards the surrounding boron powder. This central hole constitutes a major obstacle

for scaling-up the IMD wire and reduces the engineering critical current density as the overall cross-section area of the IMD wire is considered (Jie et al., 2017). In a study of Maeda et al., the localized IMD (LIMD) method which uses the coarse grained Mg powder instead of Mg rod and the cold high pressure densification (CHPD) method were tried together (Maeda et al., 2013). The use of crystalline boron powder with CHPD and LIMD methods led to the fabrication of more economical long MgB₂ wires than that of the IMD wires. A high enough J_c of 10^4 A/cm² at $T = 4.2$ K and under $B = 8$ T was achieved for this cost effective wire production. The combination of CHPD with LIMD could not provide a solution for the porosity but could densify the core region by reducing the initial empty spaces which mostly form due to insufficient compression in the conventional PIT method. A low core density is a major obstacle in order to obtain high J_c values for the *in-situ* MgB₂ wires. It is generally accepted that porosity is inevitable but the *in-situ* MgB₂ wires can be improved by increasing the active superconducting area which contributes to the grain connectivity and thus J_c .

The J_c in high magnetic fields is also enhanced by using external additives in the *in-situ* MgB₂ wires (Gao et al., 2010; Yang, 2016). The studies have shown that different types of carbon-based additives such as nano SiC, carbon nanotubes (CNTs), or nano-sized carbons are good candidates to increase the J_c in high fields but these are found to be insufficient to increase J_c in the self-magnetic field (Kim et al., 2006; Dou et al., 2006; Kim et al., 2012; Ghorbani et al., 2014). Low field J_c is important in terms of low field applications of MgB₂ wires such as magnetic resonance imaging (MRI) magnet or current leads (Zeng et al., 2007; Susner et al., 2013). It is accepted that the sintering temperature and the substitution of carbon with boron modify the flux pinning mechanism in MgB₂. In particular, SiC addition significantly improves the in-field J_c and B_{c2} but, the agglomeration of nano C is a major barrier in front of the large scale wire production. Malic acid (C₄H₆O₅) is also used as a carbon source in the MgB₂ wire production. This organic compound has the advantage that the carbon is homogeneously incorporated by the wet mixing process. The use of malic acid results in the formation of carbon-encapsulated boron that prevents agglomeration during the reaction process. The pinning properties of *in-situ* MgB₂ wires can be improved in a wider range of magnetic fields by inclusion of malic acid (Kim et al., 2006; Motaman et al., 2013).

Another factor which limits the J_c of *in-situ* MgB₂ wires is the formation of some oxide phases such as MgO between the superconducting MgB₂ grains because Mg is highly prone to oxidation (Klie et al., 2001). These insulating MgO layers can prevent the flow of current, this is known as percolation threshold, and cause a connectivity problem in the MgB₂ core structure (Yamamoto et al., 2007). On the other hand, it was found that the oxygen rich boron phases (BO_x, MgO etc.) with sizes as small as the coherence length could serve as the effective pinning centres and enhance the J_c in the presence of external magnetic field (Kim et al., 2007). Although the formation of small sized BO_x contributes to the flux pinning at inter-granular region, further increase in oxygen content causes large MgO layers that limit the number of possible current paths. The well-connected grains have a central role on further increase of the J_c because the insufficient number of current flow paths often results from the formation of excess oxide phases. Therefore, MgB₂ stoichiometry is important in terms of the dominations or reductions of O-rich secondary phases, in particular the MgO phase which occupies the inter-granular region (Zhang et al., 2015).

The studies performed on excess-Mg wire samples showed that the transport J_c could be improved up to 10 % excess-Mg ratio. Besides the J_c , it was also revealed that B_{irr} , and B_{c2} of MgB₂ wires were enhanced when an extra Mg was included (Zeng et al., 2007). However, these superconducting properties were also found to be highly dependent on the processing temperature for the excess Mg samples. A number of studies have been conducted to investigate the effect of Mg/B ratio on the properties of MgB₂ samples, but no consensus has been reached because the differences between the results of studies to reveal the effects of Mg non-stoichiometry on the superconducting properties of MgB₂ were found (Xiao et al., 2003; Jiang et al., 2007; Chen et al., 2008; Li et al., 2009). For instance, it was found that the Mg deficient samples showed better J_c 's at high magnetic fields than that of the Mg excess samples. It was reported that Mg-deficiency, even at ratios less than 1%, boosted the J_c in the presence of magnetic field. It has been suggested that variations in structural and superconducting properties due to Mg non-stoichiometry result from Mg particle size and purity, mixture homogeneity and changes in MgO formation. Therefore, it is important to improve the transport properties of MgB₂ wires with Mg/B optimization (Susner et al., 2007).

In the present thesis, we have performed transport characterization measurements on the MgB₂/Fe wire which is fabricated by an alternative technique, called Mg-coating method. This study intends to improve transport properties of MgB₂ wires under external magnetic field and contribute to the current debates on Mg non-stoichiometry in the literature. It has been revealed that the initial excess Mg level, less than 1 wt. %, induces significant positive changes on the transport properties of MgB₂/Fe wires under moderate magnetic field strengths (Karaboga et al., 2017; Yetis et al., 2019).

The rest of the thesis is organized as follows: Chapter 2 defines the aim of this thesis and explains the main idea of the study. Chapter 3 describes the superconductivity, its critical parameters, and some important theories about the superconductivity. Chapter 4 presents the fundamental properties of the MgB₂ conductor, its crystal and electronic structure, and basic superconducting properties. Chapter 5 gives information about the production and characterization methods for MgB₂ wire application. Chapter 6 includes material preparation and experimental measurement processes. In Chapter 7, experimental results are presented and the results are interpreted in the light of the structural and transport characterization measurements. Finally, some important results of the thesis are concluded in Chapter 8.

2. AIM AND SCOPE OF THE STUDY

The present study is intended to improve the transport properties of *in-situ* MgB₂/Fe wires under low and moderate external magnetic fields. A novel Mg-coating method has been proposed to achieve this goal and the main reasons for the implementation of this method are as follows.

Mg-coating method is preferred to incorporate a small amount of excess Mg into the structure homogeneously and effectively during the reaction process. The idea is to contribute to the studies on the low Mg non-stoichiometry, which significantly affects the grain connectivity. Furthermore, the external diffusion by Mg-coating method is intended to include excess Mg because the porosity is further reduced in this way.

The iron sheath is particularly preferred because of its mechanical and chemical properties. Mg-coating method is intended to prevent the formation of iron boride phases such as Fe₂B at the core/sheath interface region but, this has been partly achieved.

3. SUPERCONDUCTIVITY

3.1 Discovery of Superconductivity and Superconductors

A novel type physical phenomenon was observed in 1911 when the temperature dependent resistivity measurement of mercury element (Hg) was performed. This phenomenon was that, the resistance of the mercury had completely disappeared at a certain temperature $T_c = 4.2\text{K}$ as shown in Figure 3.1. This important observation led to the discovery of superconductivity by Dutch physicist H. K. Onnes and his assistant G. Holst in Leiden and initiated studies on superconductivity. Besides observation of superconductivity in the mercury, superconductivity around liquid helium was observed in many metals, metallic alloys and intermetallic compounds. Interestingly, the superconducting phase transition was observed in lead and tin metals, but this transition did not occur in good conductors such as gold and copper.

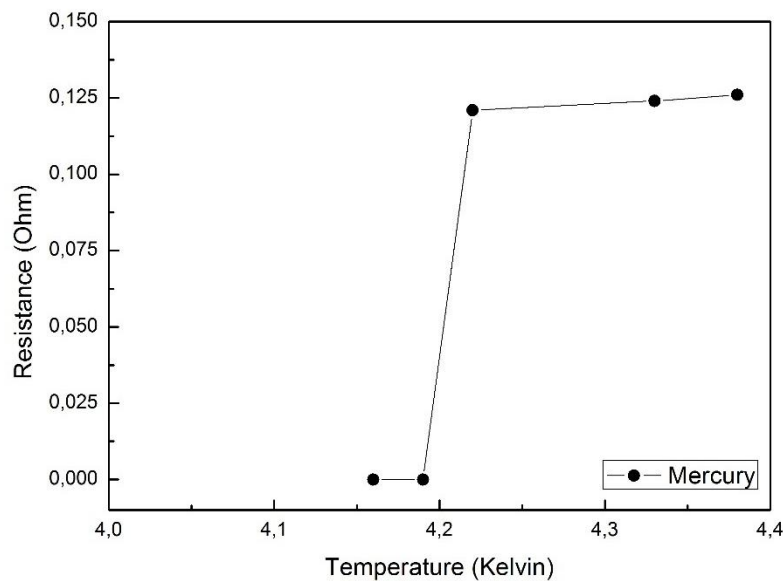


Figure 3.1. The graph represents the measurement of resistance versus temperature of a mercury rod.

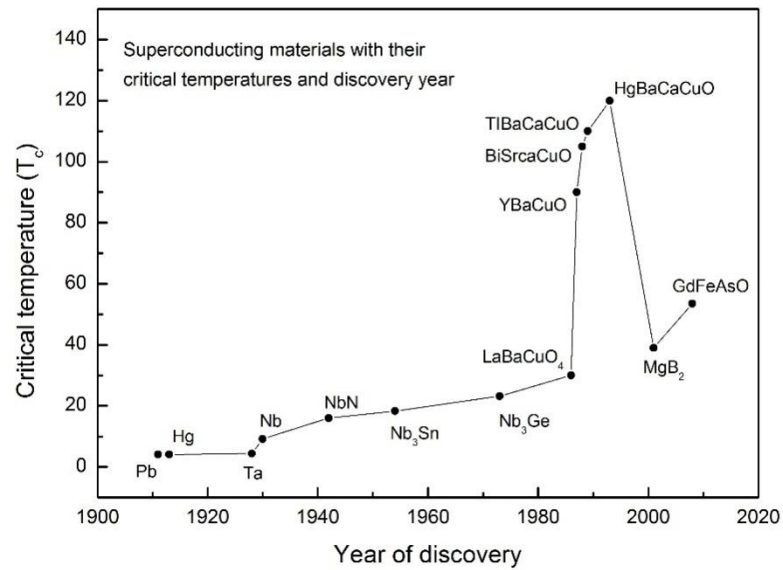


Figure 3.2. Discovery of superconducting materials with their critical temperatures (T_c).

Up to 1930, the highest critical temperature of pure elements exhibiting superconductivity was measured in Niobium (Nb) as $T_c = 9.2\text{K}$. After 1911, many scientists searched for ways to make superconductor with critical temperatures around room temperature. Figure 3.2 shows the critical temperatures of discovered compounds against date of discovery. In the 1950s and 1960s superconducting Nb alloys such as Nb₃Sn (niobium-tin) and NbTi (niobium-titanium) were found and studied. Efforts to explore superconducting materials with higher critical temperatures have resulted in the discovery of high temperature superconductors (HTSCs). In 1986, A. Müller and G. Bednorz made a real breakthrough in superconductivity at the IBM Research Laboratory. The ceramic LaBaCuO compound showed superconductivity at 30K, while normally ceramic materials were known as insulators. In the following year, researchers working at the Houston and Alabama Universities discovered the Y₁Ba₂Cu₃O₇ ceramic superconductor with a critical temperature of $T_c = 92\text{K}$. One of the reasons for the importance of this reconnaissance is the presence of a superconductor with critical temperature above the liquid nitrogen temperature of 77K. Subsequently, Bi- and Tl-based copper oxide superconducting ceramics with critical temperatures of 110K and 125K were discovered. A known highest critical temperature $T_c = 133\text{K}$ belongs to a ceramic superconductor made of mercury, barium, calcium, copper and oxygen but

higher critical temperatures are also attainable up to 164K at high pressures. In 2001, Japanese researchers found that MgB_2 , a previously known material, was superconductor at 39K. This value was well above the T_c of any elemental or binary alloy superconductors. Subsequent investigations on MgB_2 have determined that MgB_2 performs better than NbTi and Nb_3Sn in high magnetic fields. The most recently discovered superconducting group is pnictides. These iron-based superconductors were first observed in 2006. The superconductivity mechanism of pnictides with high T_c values of 50K has not been resolved yet as in high- T_c copper oxides.

3.2 Zero Electrical Resistivity and Perfect Diamagnetism

In order to classify a material as a superconductor, it is necessary that this material must have two characteristic features. It should have both zero electrical resistance under a certain critical temperature and perfect diamagnetic behavior below a certain applied magnetic field strength.

The most prominent feature of superconductivity is that the electrical resistance of a material is completely disappeared under a certain temperature known as the critical temperature. Some experiments have been carried out in order to determine if there is any small residual resistance in the superconducting state. Residual resistance can be detected by a precise test by starting a direct current flowing through a superconducting loop and observing whether the current is distorted or not. Experiments have shown that superconducting current remains stable for years in the precision of measuring equipment. This persistent current state is a characteristic of the superconductivity. It is concluded that a superconductor has a resistivity ρ less than $10^{-26}\Omega\cdot\text{m}$ and this value is about 10^{18} times less than the resistance of copper at room temperature ($10^{-8}\Omega\cdot\text{m}$). Another significant consequence of the persistent currents is that the magnetic flux which passes through a superconducting ring remains constant.

The second characteristic of a superconducting material is that the magnetic induction in the superconductor which is cooled to a temperature below the T_c in weak external magnetic field must be zero. That is, the applied external magnetic field is excluded and thus $B = 0$ inside the superconductor. This event is a natural consequence

of superconductivity and is known as the Meissner effect. The exclusion of the magnetic field is independent of whether the transition to superconductivity occurs under an applied magnetic field or in zero field.

3.3 Meissner Effect

Superconductors are unusual materials with excellent diamagnetic properties in addition to their zero electrical resistances under a certain critical temperature. Each superconducting material has a definite critical temperature and magnetic field value below which its superconductivity sustains. These temperature and field values are inter-related and beyond these critical values, the material loses its superconducting properties. When an external magnetic field is applied to a superconductor at a temperature above its critical temperature, the material will have a magnetic field almost equal to the applied magnetic field because it is not in the superconducting state. If the temperature is lowered to the superconducting state, the magnetic field lines will be pushed out of the superconductor surface and the magnetic field inside the superconductor will be zero. The superconductor has an excellent diamagnetic property on its surface by creating a magnetic field with an equal but opposite direction to the applied magnetic field.

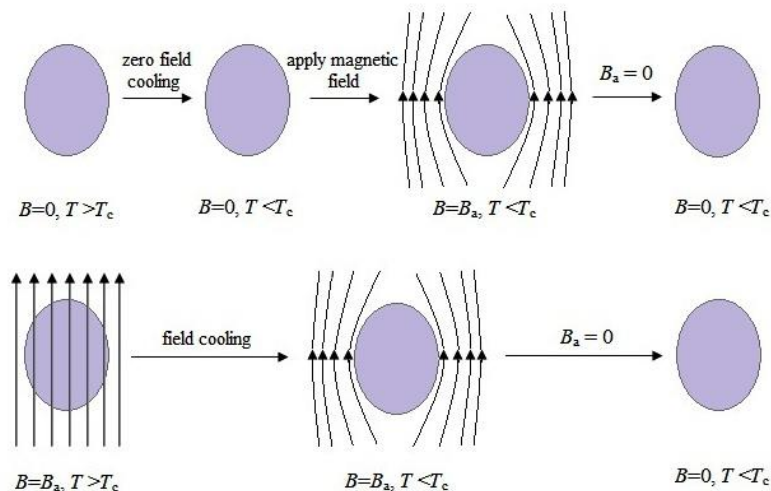


Figure 3.3. Schematic representation of Meissner effect for a superconductor under zero field-cooled and field-cooled conditions.

In Figure 3.3, the effects of the external magnetic field on a superconductor are shown. The exclusion of the magnetic field from the interior of a superconductor is known as the Meissner effect (Schmidt, 1997). This exclusion makes the magnetic field lines closer to each other on the surface of the superconductor. When the applied magnetic field is finally removed, there will be no change in the magnetic flux of the superconductor, that is $B = 0$. The difference between a superconductor and a perfect conductor occurs when they are cooled below their critical temperatures in the presence of weak applied magnetic field. In the case of field cooling process, the perfect conductor does not maintain zero internal flux state after the external field is removed, but a superconductor does, as shown in Figure 3.3.

3.4 Magnetic Properties of Superconductors

Superconductors are basically divided into two groups: Type I superconductors and type II superconductors due to their different behavior under the external magnetic field.

3.4.1 Type I Superconductors

Type I superconductors exclude magnetic fluxes up to a certain critical field (B_c) when an external magnetic field (B) is applied in the $T < T_c$ region. The magnetic induction inside the superconductor does not change as the B increases and the superconductor continues to stay in the Meissner state. However, when B is greater than a certain B_c , the magnetic field completely penetrates the sample. This magnetic field strength which completely destroys diamagnetic property of a superconductor is called the critical thermodynamic field (B_c). For a type I superconductor, the temperature dependence of B_c is almost parabolic:

$$B_c(T) \cong B_c(0) \left[1 - \left(\frac{T}{T_c} \right)^2 \right] \quad (3.1)$$

Where $B_c(0)$ is the thermodynamic critical magnetic field value at 0K. The temperature dependence of B_c is given in Figure 3.4.

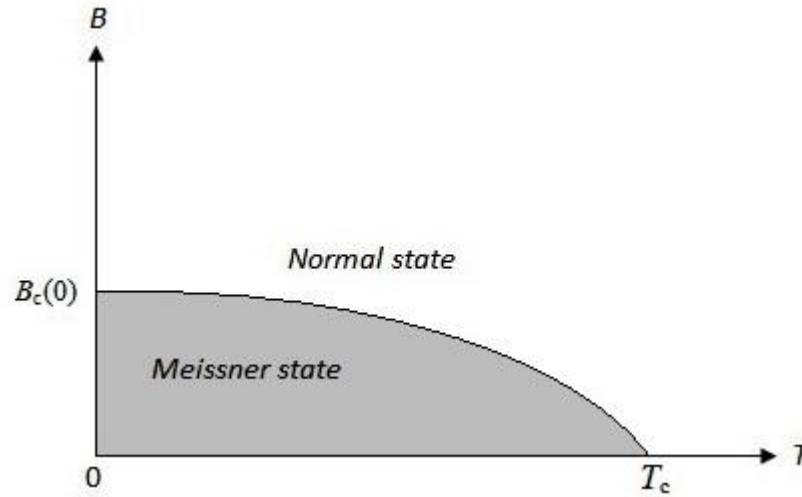


Figure 3.4. Temperature dependence of B_c for a type I superconductor. Except for Nb, pure samples of all superconducting elements exhibit type I behavior.

As shown in Figure 3.4., the superconductor is in a Meissner state with a magnetic susceptibility $\chi = -1$ as long as it is under an applied magnetic field below B_c . $\chi = -1$ is an ideal diamagnetism state which is a measure of the fact that weak magnetic fields are completely excluded from the superconductor.

3.4.2 Type II Superconductors

Type II superconductors have two critical magnetic field values such as B_{c1} and B_{c2} different from the type I superconductors. B_{c1} is called lower critical field and the magnetic flux inside the sample is completely excluded if the external field strength is below this critical value. The magnetic behavior of type II superconductors up to B_{c1} is similar to that of the type I superconductors. For an applied magnetic field in the range of B_{c1} and B_{c2} , the situation is very different for the type II superconductors. Unlike the type I superconductors, the magnetic field neither penetrates completely into the sample nor is expelled totally, instead, magnetic flux partially penetrates into the body of the sample. A mixed state, sometimes also called vortex state, in which a part of the magnetic flux penetrates the sample is established. Finally, a phase transition occurs

from the superconducting state to the normal state above the upper critical field value of B_{c2} . These phase regions are shown in Figure 3.5 for the magnetization curve of a type II superconductor as a function of magnetic field.

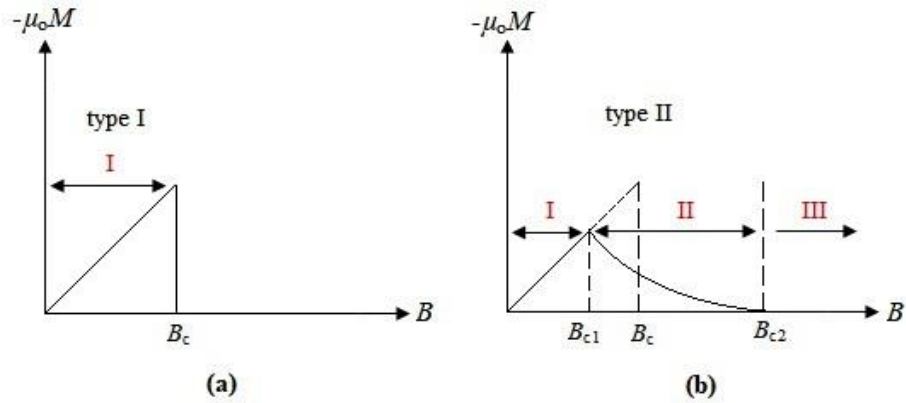


Figure 3.5. The magnetization curves of type I and type II superconductors. The phase regions are represented as I: Meissner state, II: Mixed state, and III: Normal state. The superconductivity is completely lost in the normal state.

In the range of $B_{c1} < B < B_{c2}$, the magnetic flux penetrates into the sample in a special form which is called a vortex. A vortex consists of a normal core which is surrounded by the super-currents. These super-currents circulate around the normal core such that the external magnetic field at the center is preserved. Each vortex has a flux quanta of $\Phi_0 = h/2e$. Here h is the Planck's constant and e is the charge of electron.

3.5 Critical Parameters of Superconductors

The critical parameters of superconductivity are critical temperature (T_c), critical current density (J_c), and thermodynamic critical magnetic field (B_c). The superconducting state can be destroyed if one of these critical limits are exceeded in a type I superconductor. There are also lower critical magnetic field (B_{c1}) and upper critical field (B_{c2}) values for a type II superconductor which has both normal and superconducting regions between these critical limits.

3.5.1 Critical Temperature (T_c)

The resistivity of a metallic conductor decreases with decreasing of temperature. The total resistivity of a metallic conductor is explained empirically by Matthiessen's rule as given in Equation (3.2)

$$\rho_{total} = \rho_{thermal} + \rho_{imperfections} \quad (3.2)$$

Where, $\rho_{thermal}$ and $\rho_{imperfections}$ are the resistivities from thermal agitations and imperfections in the crystal. It is seen from Figure 3.6 that the resistivity of a superconductor suddenly drops to zero resistivity level at a temperature T_c but, the electrical resistivity of an impure metal gradually decreases and reaches to a non-zero value which is called residual resistivity at 0K.

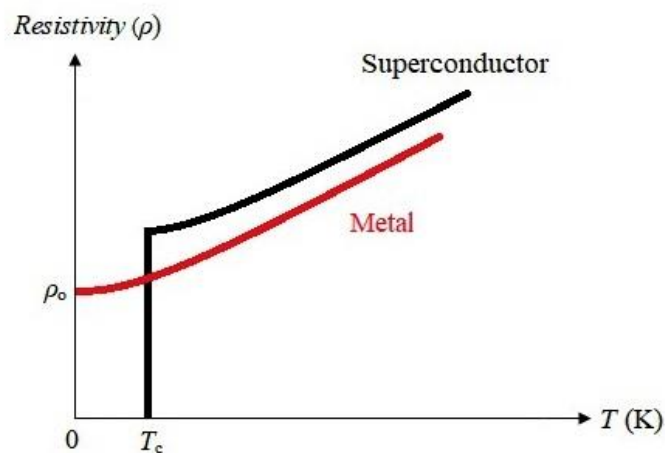


Figure 3.6. Temperature dependence of electrical resistivity of metal and a superconductor. T_c is the critical temperature of a superconductor and ρ_0 is the residual resistivity of a metal at 0K. A second order phase transition from normal state to superconducting state is observed below the T_c .

3.5.2 Critical Magnetic Field (B_c)

The free energy of a normal conductor (G_n) is reduced if this conductor becomes a superconducting at a certain T_c , that is $G_s < G_n$ where G_s is the free energy per unit volume for a superconductor below T_c . In the presence of external magnetic field B , an increase in the free energy of a superconductor occurs as given in Equation (3.3)

$$G_s(B) = G_s(0) + \frac{\mu_0}{2} B^2 \quad (3.3)$$

The free energy of the superconductor increases with increase of the external magnetic field and equals the free energy of a normal conductor at a certain field B_c .

$$G_n = G_s(0) + \frac{\mu_0}{2} B_c^2 \quad (3.4)$$

If the B_c value of a superconductor is exceeded, a superconductor can be turned into a normal conductor even below the T_c value as in Equation (3.4).

3.5.3 Critical Current Density (J_c)

The maximum current that a superconductor can carry without resistance is called the critical current density. An applied current which is higher than the critical current (I_c) leads to the superconductor to revert to its normal state. The I_c is closely related to the B_c value and is simply defined by the equation $I_c = 2\pi r B_c / \mu_0$ for a superconductor wire with a radius r . An external magnetic field or a current passing through the sample may contribute to a magnetic field at the surface of a superconductor. This field will cause the screening currents circulate on the surface of the superconductor. When the vector sum of applied current and screening currents exceeds the critical current of the superconductor, a transition to the normal state is observed. This means that the magnetic field on the surface exceeds the critical field strength.

Type-I superconductors have very low critical magnetic field values which make them unsuitable to be used in practical applications. When a current is passed through a

type-I superconducting wire, the critical field B_c is easily exceeded and the wire becomes normal. In a type-II superconductor, above the B_{c1} , the vortices nucleate in the sample, and these vortices are forced to move because of a Lorentz force as a whole ($\vec{F}_L = \vec{J} \times \vec{B}$) due to an applied current. The motion of vortices create an electric field according to the Faraday's law ($\vec{\nabla} \times \vec{E} = -\frac{\partial \vec{B}}{\partial t}$), and the electrical resistance, in other words energy dissipation occurs. The flux motion can be prevented in the presence of crystal defects which behave as pinning centers, if the Lorentz force is lower than the pinning force ($F_p = J_c B$). J_c is called the depinning or critical current density. The J_c is an extrinsic quantity which depends on the flux pinning properties of the sample, temperature, magnetic field and can vary locally.

3.6 London Theory

The phenomenon of flux penetration through the superconductor or Meissner effect was first explained by H. London and F. London. London brothers in 1935 proposed a two fluid model of superconductors. According to the model, total electron density of the superconductors n_T can be written as

$$n_T = n_s + n_n \quad (3.5)$$

The sum of n_s is the super electron density and n_n is the normal electron density. For superfluid electrons, Newton's second law of motion can be written as

$$m \frac{d\vec{v}_s}{dt} = -e\vec{E} \quad (3.6)$$

And the super current density

$$\vec{J}_s = -n_s e \vec{v}_s \quad (3.7)$$

Where \vec{E} is the electric field inside the superconductor, if the J_s term in Equation (3.7) is differentiated with respect to time and then used in the Equation (3.6)

$$\vec{E} = \frac{m}{n_s e^2} \frac{d\vec{J}_s}{dt} \quad (3.8)$$

So the London's first equation which gives the value of electric field is obtained. When the curl of both sides in Equation (3.8) is taken and Faraday's induction law is used, then

$$\vec{\nabla} \times \vec{J}_s = -\frac{n_s e^2}{m} \vec{B} \quad (3.9)$$

Equation (3.9) is known as London's second equation.

3.6.1 London Penetration Depth

The first and second London equations are used to explain flux penetration (Meissner effect) through the superconductor. If the curl of the differential form of Ampere's law is taken, we get

$$\vec{\nabla} \times \vec{\nabla} \times \vec{B} = \mu_o (\vec{\nabla} \times \vec{J}_s) \quad (3.10)$$

By using the Equation (3.9) and Gauss Law for magnetism from Maxwell equations

$\vec{\nabla} \cdot \vec{B} = 0$, the Equation (3.10) becomes

$$\nabla^2 \vec{B} = \frac{\vec{B}}{\lambda_L^2} \quad (3.11)$$

Where λ_L is known as London's penetration depth and $\lambda_L = \left(\frac{m}{\mu_o n_s e^2}\right)^{1/2}$ and m is the mass of electron. The solution of differential equation (Equation (3.10)) in one dimension is equal to $B(x) = B(0)e^{-x/\lambda}$, where $B(0)$ is the magnetic field at the surface of a superconductor. This shows that the external magnetic field penetrates into the superconductor with exponential attenuation. However, the exponential decay of the magnetic field does not apply to type I superconductors, because the λ_L value of the type I superconductors is so small that the magnetic field changes cannot be explained by the London's local electrodynamics approach. A non-local electrodynamics of Type I

superconductors was proposed by Pippard and it predicts that the magnetic field penetrates deeper than the λ_L derived by local London electrodynamics.

3.7 Ginzburg Landau Theory

The Ginzburg-Landau (GL) theory is a phenomenological quantum theory of superconductivity which explains the distinction between the type I and type II superconductors theoretically. The GL theory is based on the Landau's theory on second-order phase transitions and showed that the Helmholtz free energy difference between the superconducting and the normal states could be expanded in powers of the order parameter near the T_c . The spatially varying wave function of super electrons $\psi(\vec{r})$ is anticipated as the order parameter. The $|\psi(\vec{r})|^2$ is a measure of super electron density and $|\psi(\vec{r})|^2$ is zero above the T_c and non-zero at a temperature below the T_c .

$$F_s = F_N + \alpha|\psi|^2 + \frac{\beta}{2}|\psi|^4 + \frac{1}{2m^*} \left| (-i\hbar\vec{\nabla}\psi - \frac{e^*}{c}\vec{A})\psi \right|^2 + \frac{B^2}{8\pi} \quad (3.12)$$

Where $\psi(\vec{r}) = \left(\frac{n_s(\vec{r})}{2}\right)^{1/2} e^{i\theta}$ and $n_s(\vec{r})$ is the local density of super electrons. θ is the phase term, \hbar equals to $h/2\pi$, m^* is the effective mass, and e^* is the effective charge of the super electrons. \vec{A} and $\vec{B} = \vec{\nabla} \times \vec{A}$ are the local vector potential and the local magnetic field, respectively. α and β and are phenomenological expansion coefficients.

3.7.1 Ginzburg-Landau Parameter

The London penetration depth (λ_L) which is also provided by GL theory and the coherence length (ξ_{GL}) which defines spatial variations of the order parameter $\psi(\vec{r})$ near a normal-superconductor (NS) boundary are two characteristic lengths in superconductivity. The ratio of these two characteristic lengths are defined as GL parameter (κ) in the framework of GL theory such as

$$\kappa = \frac{\lambda_L}{\xi_{GL}} \quad (3.13)$$

Where $\xi_{GL} = \sqrt{\frac{\hbar^2}{2m|\alpha|}}$. It was predicted from the solutions of GL equations that the superconductors could be classified according to their κ values: A superconductor is of type I if $\kappa < \frac{1}{\sqrt{2}}$ and type II if $\kappa > \frac{1}{\sqrt{2}}$. In 1957, A. A. Abrikosov found out that the surface energy between normal and superconducting interface region could also have a negative value that is $\sigma_{ns} < 0$, and revealed the existence of a new type of superconductors which is called type II superconductors (Abrikosov, 1957).

3.8 BCS Theory

The quantum explanation of superconductivity in conventional superconductors was first proposed by Bardeen, Cooper, and Schrieffer (BCS) in 1957 that is 46 years after the discovery of superconductivity (Bardeen et al., 1957). The BCS model briefly described the mechanism underlying the superconductivity of a metal in terms of the weak interaction between electrons and phonons. It demonstrated that electron-phonon interaction leads to an attraction between two electrons near the Fermi level which results in the formation of Cooper pairs. A Cooper pair has a zero spin and obeys the Bose-Einstein statistics. Below the T_c , all Cooper pairs condensate to a lowest energy state and they transport the current without energy dissipation.

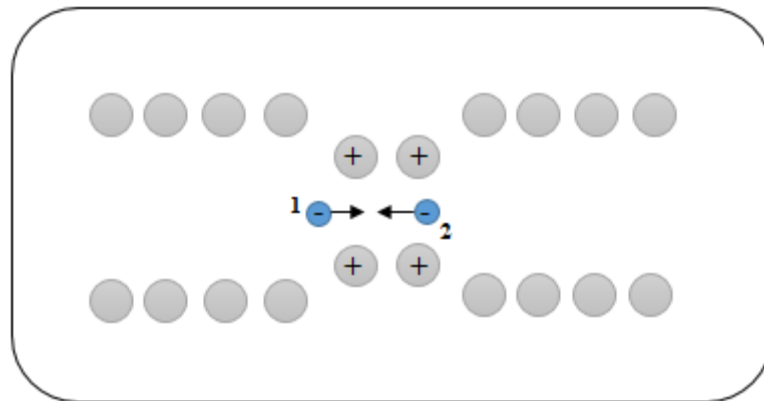


Figure 3.7. The electron-phonon interaction. The electron 1 and electron 2 form a Cooper pair.

The BCS theory contains an important parameter which is coherence length, ξ_0 , defined as the maximum distance which the coherent electron-electron interactions of Cooper pairs can get. It depends on the Fermi velocity and the energy gap:

$$\xi_0 = \frac{\hbar v_f}{\pi \Delta_0} \quad (3.14)$$

Δ_0 is an energy gap which is required amount of energy to destroy the superconducting state and make it normal, here v_f represents Fermi velocity.



4. MAGNESIUM DIBORIDE SUPERCONDUCTOR

4.1 Discovery of MgB₂

The superconductivity was first discovered in the MgB₂ material with a transition temperature T_c at 39K by Japanese researchers in 2001 (Akimitsu et al, 2001). As a result of this discovery, the transition temperature of the MgB₂ has been accepted as the highest value among the other inter-metallic compounds. Many scientists have worked on the crystal and electronic structures of the MgB₂ material and many studies have been carried on single crystal, bulk sample, thin film, tape and thin wire forms of MgB₂ to investigate its basic properties and its applicability to the technology (Flükiger et al, 2003).

4.2 Crystal Structure of MgB₂

Magnesium diboride is an inter-metallic compound which has a simple hexagonal AlB₂ type crystal structure with a p6/mmm space group as other diborides. The lattice parameters of MgB₂ are $a = b = 3.08\text{\AA}$ and $c = 3.51\text{\AA}$ (Kortus et al., 2001).

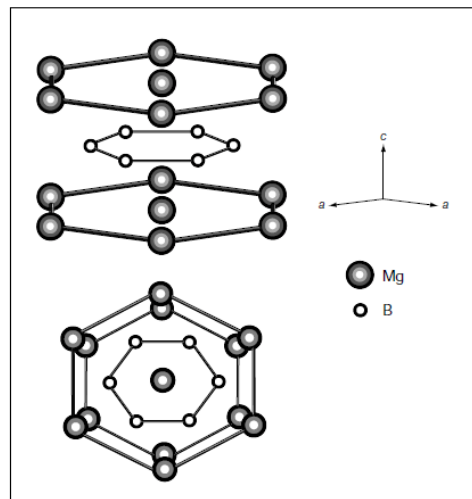


Figure 4.1. The crystal structure of magnesium diboride superconductor (Akimitsu et al., 2001).

MgB₂ has a layered structure which contains magnesium and boron layers, where the boron atoms aligned in graphite-like honeycomb planes which are separated by hexagonal layers of magnesium atoms as shown in Figure 4.1. The distance between the boron atoms in the *ab*-plane is much smaller than in the *c*-direction. The inter-atomic distances are equal to 1.780Å between the B-B layers and 3.084Å between the Mg-Mg layers. Superconductivity with a high transition temperature is achieved due to strong electron-phonon interactions with high vibrational frequencies of light B atoms in MgB₂. (Ravindran et al., 2001). Thus, the magnesium diboride has the highest value of the critical temperature than the other inter-metallic compounds.

4.3 Electronic Structure of MgB₂

The electronic band structure of MgB₂ superconductor has an intrinsic property which is defined as two band superconductivity. This phenomenon was observed in the MgB₂ superconductor with its 3D π -bands and 2D σ -bands (Wang et al., 2001). The 2D covalent σ -bands occur owing to the boron $p_{x,y}$ and $2s$ orbital which form sp^2 hybridization. The three dimensional (3D) metallic π -bands are formed by boron p_z orbital. Both holes and electrons as the charge carriers comprise in the π -band. Magnesium and boron atoms form an ionic bond whereof the Mg atoms donate their valence electrons to the Boron layer and fully ionize (Bunzea and Yamashita, 2001). Mainly, the Fermi surface is derived from boron orbital because the boron bands are more effective in the formation of the valence bands in MgB₂ than magnesium. Many researchers proposed that the metallic boron layers have a major role in the superconducting feature of the MgB₂ (An and Pickett, 2001; Kortus et al., 2001).

When the density of states (DOS) and the band structure of MgB₂ are scrutinized, there is a major electron transfer from the Mg atom to the two B atoms. The contribution of the B p -orbital is dominant on the overall shape of the total density of states (Armstrong et al., 1979). Additionally, electronic structure calculations demonstrate that although magnesium atoms have weak bonding, there is a strong covalent bond between boron atoms which causes a strong electron-phonon interaction due to the strong coupling between the quasi-two-dimensional B σ -bands and E_{2g} phonon modes.

4.4 Superconducting Mechanism in MgB₂

Several experimental and theoretical studies have been conducted on how the superconductivity mechanism works in the MgB₂. The studies revealed that the high transition temperature of MgB₂ arises from its intrinsic properties such as strong bonding, reasonable Fermi level density of states and high phonon frequency. The high transition temperature of the MgB₂ is also attributed to 2D character of the boron Fermi surface (An and Pickett, 2001). The superconductivity of MgB₂ can be explained by BCS theory in terms of the electron-phonon coupling which carries the molecular mass, the phonon frequency and the Fermi level density of states. The boron isotope effect is also another indicator that MgB₂ is a BCS superconductor. The MgB₂ superconductor is called Type-1.5 superconductor due to its strange magnetic character which is resulted from its two-band nature. MgB₂ has both type-I and type-II superconducting behaviors, so that the type-I superconductivity occurs due to the π -bands and type-II superconductivity is due to the σ -bands in MgB₂ (Moshchalkov et al., 2009).

4.5 Anisotropy (γ)

Anisotropy can be defined by the ratio of effective mass of the electron in different crystal directions. An electron can move more easily in some certain direction than other crystal directions (Sheahen, 2002). The ratio of effective mass in c and a axis is given by

$$\gamma = \sqrt{m_c^*/m_a^*} \quad (4.1)$$

The anisotropy exists in several superconducting parameters of MgB₂ such as coherence length ξ , penetration depth λ , the upper critical field B_{c2} and the lower critical field B_{c1} .

The results from the crystal band structure calculations of MgB₂ show that it has a quite anisotropic electronic band nature. The theoretical studies upon the Fermi surface of the MgB₂ reported that σ -bands are quite anisotropic and π -bands are more isotropic

(Choi et al., 2002). The anisotropy in the superconducting state is defined by the standard anisotropic GL theory, such as

$$\gamma = \sqrt{\frac{m_c^*}{m_{ab}^*}} = \frac{\lambda_c}{\lambda_{ab}} = \frac{\xi_{ab}}{\xi_c} = \frac{B_{c2}^{llab}}{B_{c2}^{llc}} \quad (4.2)$$

Here m^* is the GL effective mass. $\parallel c$ is used for the case where the external magnetic field B is parallel to c -axis. However, it was demonstrated that the anisotropic properties of MgB₂ could not be explained by the anisotropic GL theory (Koshelev et al., 2004).

Many values have been reported about the anisotropy of MgB₂ superconductors produced in the form of thin film, polycrystalline, and single crystalline forms. The anisotropy ratio of B_{c2} ($\gamma = B_{c2}^{ab}/B_{c2}^c$) was reported as 2.6 for MgB₂ single crystals (Xu et al., 2001). For the aligned crystalline samples, anisotropy ratio was determined within the range of 1.6 to 1.9 as a function of temperature. The anisotropic ratio over the critical current density was assessed as approximately 1.5 by means of Bean's model (De Lima and Cardoso, 2003). M. Angst et al. revealed that the anisotropy of MgB₂ is a temperature and the magnetic field dependent quantity. They showed that γ is decreasing from 6 to 2.8 when the temperature is increased from 15K to 35K. The anisotropy of coherence and penetration lengths is linearly dependent on the magnetic field in the vicinity of the transition temperature at low fields (Angst et al., 2002). The magnetic field dependence of the anisotropies of characteristic lengths in MgB₂ reflects the anisotropy of different bands (Zehetmayer, 2013).

4.6 Isotope Effect

The isotope effect was discovered for Hg element in 1950 by E. Maxwell, C. Reynolds and his co-researchers. The isotope effect is an indicator of the phonon-mediated superconductivity. The vibrations in the crystal lattice have a crucial role in terms of the isotope effect. The isotope effect is formulated by the relation $T_c \propto M^a$ where

M is the atomic mass of the element. The isotope coefficient α was obtained close to 0.5 for Hg, Pb, and Sn (Maxwell 1950; Reynolds et al., 1950; Garland 1963).

Table 4.1. The isotope effect coefficient values for some elements (Mourachkine, 2004).

Element	α
Mg	0.5
Sn	0.46
Mo	0.33
Re	0.4
Zr	0 (± 0.05)

The studies performed on the Mg^{10}B_2 and Mg^{11}B_2 revealed the existence of boron isotope effect with an isotope coefficient of $\alpha = 0.26 \pm 0.03$ and 1K shift at T_c . This finding demonstrated that MgB_2 is a BCS superconductor and the boron E_{2g} phonon modes are effective in superconductivity of MgB_2 (Bud'ko et al., 2001). The total reduced isotope coefficient was found to be $\alpha = 0.32$. The α_{Mg} of the Mg isotope effect was found to be very small at 0.02 (1), indicating that the vibration frequencies of Mg atoms have virtually no effect on T_c (Hinks et al., 2001).

4.7 Grain Connectivity, Porosity and Weak-Link

The grain connectivity has a significant role on the superconducting properties of MgB_2 superconductor. Several studies demonstrated that the grain size, the density of the grains and the pinning mechanism at the grain boundaries are effective on the critical current density of MgB_2 (Mikheenko et al., 2007; Martínez et al., 2007; Tatiana et al., 2017). The various researches have shown that the grain size changes between 10nm to 200nm in MgB_2 (Hata et al., 2006; Jiang et al., 2005). The critical current density is increased in the presence of dense grains with strong links between the grain boundaries. In MgB_2 , the strong links are present in the natural grain boundaries which are transparent. The weak link problem usually occurring in high- T_c superconductors is almost absent in polycrystalline MgB_2 (Matsushita et al., 2008). The natural grain boundaries are considered to be the source of pinning centers in MgB_2 superconductors.

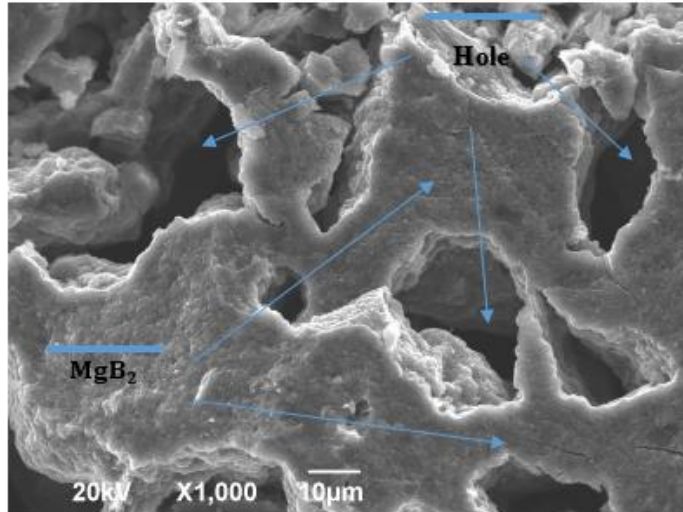


Figure 4.2. Porous microstructure in an *in-situ* MgB₂ superconducting wire (SEM analysis).

The porous microstructure occurs due to the reaction of Mg with B for an *in-situ* processed MgB₂ sample as shown in Figure 4.2. The initial mass density is about 65% of the MgB₂ for an *in-situ* PIT processed wire but the density is further reduced due to the volume contraction during the reaction. The final mass density is about 50% of theoretical density of MgB₂ in wires (Collings et al., 2008; Jie et al., 2017).

5. MgB₂ WIRE AND ITS DEVELOPMENT

5.1 Fabrication Techniques

5.1.1 PIT and CTFF Methods

The superconducting MgB₂ wires are mostly fabricated by Powder-In-Tube (PIT) or Continuous Tube Filling and Forming (CTFF) methods (Glowacki et al., 2001; Tomsic et al., 2007; Ma et al., 2008). In the PIT method, one end of an empty pre-cleaned metallic tube is first closed by an appropriate material (lead, aluminum, or etc.) and then the inside of the empty tube is filled with the powder mixture to be used. Finally, the open end of the filled tube is sealed and the tube is made ready to be deformed to the wire form. The CTFF method designed to increase the filling density is based on continuously pouring the precursor powder on a metallic strip and folding it into a tubular form. The overlap-closed tube is then placed into a metallic (mostly copper) tube which is used as a stabilizer. The PIT method is an inclusive technique that involves almost all possible filling methods.

If the precursor powder is reacted before loading the powder into metal tubes, this process is called *ex-situ*. The PIT method can also be applied so that the mixture of Mg and B, called *in-situ*, is filled into the tube without reaction. The *in-situ* processed MgB₂ wire is more open to developments in terms of its usage in superconducting technologies. It requires a lower reaction temperature, and is suitable for adding dopants or other chemicals in order to improve its current carrying capacity in the presence of high magnetic fields.

5.1.2 IMD Method

A new fabrication route was proposed by Giunchi et al. in which a uniform Mg rod was inserted into the center of a metallic tube and B powder was filled in the gap between the Mg rod and the tube (Giunchi et al., 2003). This technique is known as the internal magnesium diffusion technique (IMD) and is based on the formation of a high

J_c MgB₂ layer by diffusion of Mg into B at the core/sheath interface region. Disadvantage of the IMD method is the formation of a hole at the center along the wire. The infiltration of Mg into the B causes a significant gap left behind and reduces the engineering critical current density J_{ce} which is determined by dividing I_c to the total cross-sectional area of the wire. The combination of the IMD method with some factors, such as the optimal precursor B powder and the selection of effective additives, resulted in the generation of a high J_c second generation MgB₂ wire (Hur et al., 2008). Excellent transport properties reported for short IMD wires have not been realized for long lengths yet, efforts to achieve this aim are still in progress (Wang et al., 2017).

5.1.3 HIP and CHPD Methods

Disadvantages of *in-situ* PIT processed MgB₂ wires are the high porosity and weak connectivity between grains. Although the IMD method has some advantage over the conventional PIT method, porosity still occurs due to the reaction of Mg with boron environment. The *in-situ* processed wire core has a lower density of precursor powder than that of the pre-reacted or *ex-situ* processed MgB₂ wire core. Porosity in the core of *in-situ* MgB₂ wires is higher because the reaction of Mg with B which yields MgB₂ causes a density contraction in which the final core density decreases up to 50% of theoretical density (2.62g.cm⁻³). Densification in the core of PIT MgB₂ wires in terms of grain connectivity and porous structure has been widely investigated. The hot isostatic pressure (HIP) method (Gajda et al., 2018), in which the reaction is completed under high pressure, significantly increases the density of the MgB₂ core, but this technique can only be applied in short wire samples. On the other hand, the cold high pressure densification (CHPD) method is applicable at long length scales (Hossain et al., 2014) and makes the starting Mg+2B *in-situ* wire core denser than the conventional *in-situ* PIT method, but this method does not improve core density and reduce porosity as much as HIP process does.

5.1.4 PeIT Method

Recently, an alternative approach to PIT method is proposed (Akdogan et al., 2015) in order to increase the initial filling density of the precursor *in-situ* Mg+2B powder inside the metallic iron tube as shown in Figure 5.1. The pellet-in-tube (PeIT) method increases initial filling density up to 60% of theoretical mass density of MgB₂ phase. It provides an important improvement for higher core density even though cannot eliminate the formation of porous structure completely. The most effective role of this method in the production of long-scale wires is that the starting powder is more uniformly filled along the tube in the PeIT method in comparison with powder filling (Karaboga et al., 2018).

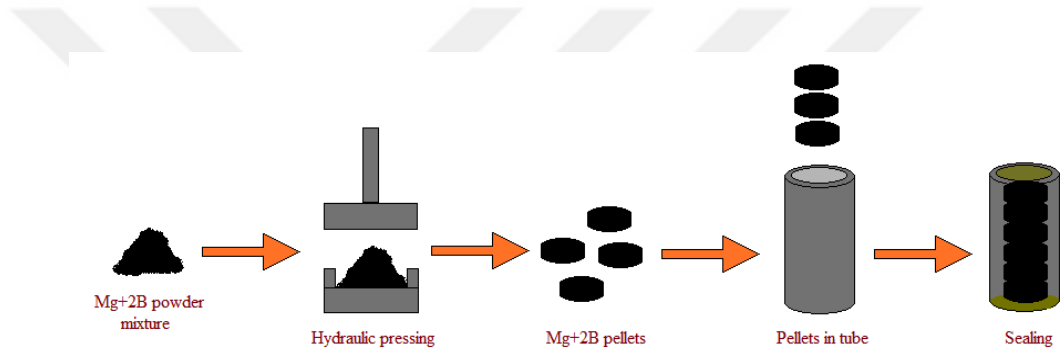


Figure 5.1. *In-situ* pellet-in-tube (PeIT) method for MgB₂/Fe wire fabrication.

5.2 Mechanical Properties

The choice of sheath material should meet the requirements of low mass density, low cost, high availability, chemical compatibility (being nonreactive with MgB₂, B, and Mg during the sintering process), appropriate mechanical strength and hardness/ductility for cold work during wire drawing. Iron (Fe), stainless steel (SS), monel, nickel (Ni), copper (Cu), silver (Ag), niobium (Nb), tantalum (Ta), titanium (Ti) and even aluminum (Al) have been tried as sheath material for producing PIT MgB₂ wires and tapes. Every material choice has its advantages and disadvantages together. The most appropriate decision will depend on the type of application. Stainless steel, niobium and monel are difficult to machine, and silver, niobium and monel are expensive. Copper and nickel are ductile but reactivity is an obstacle. For *in-situ* process, the use of iron as a chemical barrier lowers the initial cost, but diffusion of

boron into the Fe sheath may form Fe₂B layer at the metal/core interface region at relatively high synthesis temperatures (Schlachter et al., 2006; Kováč et al., 2006).

5.3 Transport Characterization Techniques

Transport properties of MgB₂ wires are mostly characterized by means of resistivity measurements (ρ - T) and current-voltage (I - V) measurements as a function of external magnetic field and operating temperature.

5.3.1 Resistivity and Connectivity Analysis

A four probe measurement method is employed in order to measure the resistance of MgB₂ wires in the presence of external or zero magnetic fields as a function of temperature. A DC current is applied for the (ρ - T) measurement and the upper critical field (B_{c2}) and irreversible critical field (B_{irr}) can be determined by 10% and 90% of normal state resistivity criteria. The resistivity and connectivity analysis of the wire samples can be made from the (ρ - T) curve after stripping off the metallic sheath from the MgB₂ core. The essential factors which influence directly the critical current density in MgB₂ wires are coupling strength between the grains and flux pinning mechanism at the grain boundaries. The porosity and the formation of oxide layers caused by heat treatment of *in-situ* MgB₂ wires restrict the current paths. The voids together with the insulating oxide layers accumulated at the grain boundaries cause the percolation problem for the current flow between the superconducting grains. The Rowell connectivity analysis describes the correlation between the electrical resistivity and effective current carrying cross sectional area of the MgB₂ sample (Rowell, 2003). The active cross-sectional area fraction (A_F) is estimated as

$$A_F = \Delta\rho_{ideal} / (\rho_{300K} - \rho_{40K}). \quad (5.1)$$

Here the ρ_{300K} is the resistivity at room temperature, ρ_{40K} is the resistivity just above the transition temperature of the MgB₂ sample. $\Delta\rho_{ideal}$ is the change in resistivity which is accepted as 4.3 $\mu\Omega$.cm for a single crystal of MgB₂ and 7.3 $\mu\Omega$.cm for a fully

dense MgB₂ filament (Jiang et al., 2006; Matsushita et al., 2008). If the cross-sectional area is reduced, an increase in resistivity of MgB₂ sample which leads to a proportional decrease at J_c is expected. MgB₂ is known as the superconductor with a relatively low normal state resistivity, with respect to the Nb based (NbTi, Nb₃Sn) conventional superconductors, and this case is very important in terms of its quench characteristics for magnet applications. Therefore, it is also important to determine the residual resistivity ratio ($RRR = \rho_{300K}/\rho_{40K}$) of MgB₂ since variations in RRR are thought to be directly related with the grain connectivity (Chauhan et al., 2010).

5.3.2 Transport J_c and Flux Pinning Mechanism

The n -value of the MgB₂ wire has an important role in understanding its current decay properties under the magnetic field (Li et al., 2012). It is determined by fitting of E vs. J characteristics of the wire samples to a power-law relation, $E \sim (J)^n$. It is commonly accepted that the use of MgB₂ conductor for a magnet design which operates in the persistent mode requires a high n -value. The n -value is a temperature and magnetic field dependent quantity and $n = 10$ -20 is an acceptable range for low field application of MgB₂ wires when operating at temperatures about 20K. It is necessary to obtain highly uniform microstructure in the MgB₂ wire core for a superconducting magnet operating in persistent mode. Thus the correlation between the J_c and the n -value should be determined in detail (Kim et al., 2010; Motaman et al., 2014).

5.4 Applications of MgB₂ Wires

Following the discovery of superconductivity in 1911, the use of excellent conductivity in practical applications was the target for researchers. This target has come to life with the discovery of type II superconductors which are capable of maintaining a significant amount of electric current under high magnetic fields. The most widely used commercial superconductors are NbTi and Nb₃Sn low temperature superconductors. NbTi superconductors are widely used in low-field electromagnets of magnetic resonance imaging (MRI) devices and have $T_c = 9.2K$ and $B_{c2}(4.2K) = 10$ -12T. The

Nb₃Sn superconductors have higher critical temperature and critical magnetic field values ($T_c = 18\text{K}$ and $B_{c2}(0) = 25\text{T}$) than NbTi. However, the use of Nb₃Sn increases the cost at low field electromagnet applications due to its fragile, stress-sensitive and difficult manufacturing. Today, the biggest disadvantage of these two low-temperature superconductors is that they can be operated at liquid helium (LHe) temperature, which increases costs considerably. This will be more important in the future as helium prices are increasing. Recently discovered FeAs-based materials have high transition temperatures ($T_c = 26\text{-}57\text{K}$) and fairly high critical magnetic fields ($B_{c2} = 20\text{T-}100\text{T}$), but it is very difficult to produce high-quality wires or tapes from these materials due to the presence of weak links between the grains. Similarly, the high costs of BSCCO (Bi-2212, Bi-2223) and YBCO (Y123) superconductors as well as their unfavorable properties such as high anisotropy, weak links, ac loss etc. cause undesirable factors in magnet fabrication (Seidel, 2015)

In the technological applications of the superconductivity, the MgB₂ superconductor is targeted because of it has a high potential in commercial applications. MgB₂ superconductors, besides their low cost, are advantageous due to their several intrinsic properties like low mass density, low anisotropy, high critical current density, and having the high critical temperature ($T_c = 39\text{K}$) in comparison with the conventional superconductors. Moreover, for practical applications, one of the significant features of MgB₂ is that these materials can operate at temperatures in the range of 20-30K, and, this temperature range can be achieved by means of modern cryocooler systems. Possible applications for MgB₂ superconductors, could be the magnetic resonance imaging (MRI) devices (Park et al., 2012), the superconducting wind turbine (Nam et al., 2018), fault current limiters (FCL) (Ye et al., 2007), superconducting magnetic energy storage devices (SMES) (Atomura et al., 2012), and transformers (Hascicek et al., 2009).

6. EXPERIMENTAL SETUP

6.1 Internal Magnesium Coating Method

A large grained magnesium powder, having a purity of 99% and particle sizes of 149-74 μm (Pavezyum), was coated to the internal surface of Fe tube by using an evaporation method. A small amount of Mg powder was weighed and filled into a pre-cleaned Fe tube which had already been sealed by aluminum foil from one of its ends. This filled Fe tube was placed into a bore of the vertical furnace in Figure 6.1 and then the bore was continuously evacuated and filled with argon gas until the temperature reaches 200°C. Thereafter, argon gas was again introduced into the bore after evacuation and the furnace temperature was increased up to 600°C under 1.5 bar gas pressure. As a final process, a final evacuation process was applied and temperature of the furnace was kept at 600°C for an hour and a thin layer of Mg on internal wall of Fe tube was achieved. The system was cooled to room temperature under 2 bar argon pressure. Any wire sample fabricated using the present method is called Mg-coated sample.



Figure 6.1. A vertical furnace and experimental set up for magnesium coating process.

6.2 Preparation of *in-situ* Mg+2B Powder

The initial Mg+2B powder was obtained from Mg powder (Purity: 99%, particle sizes 149-74 μm (PVZ)) and a mixture of boron powders containing equal amounts of amorphous boron (PVZ Boron 95, 95-97%, particle sizes $<1 \mu\text{m}$) and amorphous nano boron (Karaboga et al., 2017). The stoichiometric Mg+2B powder was ball-milled by different sized agate balls (mass ratio has equal 1:4) in argon atmosphere for 3 hours. Excess-Mg powders were prepared by adding 1wt. % and 5wt. % magnesium to the stoichiometric Mg+2B powder. The same ball-milling procedure was also followed for the preparation of non-stoichiometric powders (see Figure 6.2).

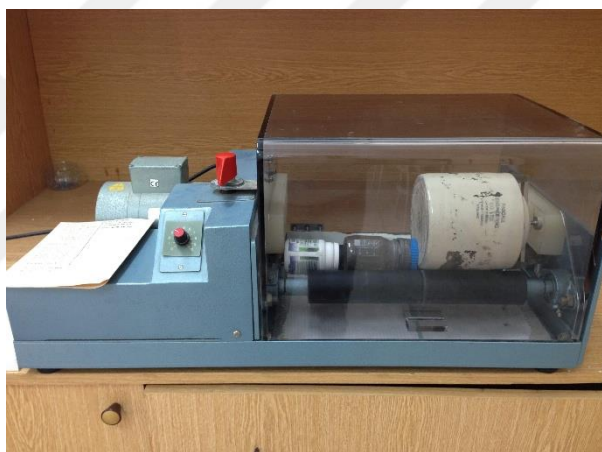


Figure 6.2. Ball milling machine which is used to obtain homogeneous mixture of stoichiometric and non-stoichiometric Mg+2B powders.

The *in-situ* MgB₂/Fe superconducting wires were fabricated by using pellet-in-tube (PeIT) and powder-in-tube (PIT) methods for stoichiometric and non-stoichiometric Mg+2B powder mixtures. The previously prepared homogeneous Mg+2B powder mixtures were used in pellet production. Mg+2B pellets were produced by using a hydraulic press in which 3 tones were applied to compress powder mixture for a short period of time. In this process, the pellets were produced with diameter of 8.8 mm as shown in Figure 6.3 and each pellet was carefully placed into the iron tube via the vacuum pipe to complete the PeIT method which was used to increase initial powder filling density and uniformity.

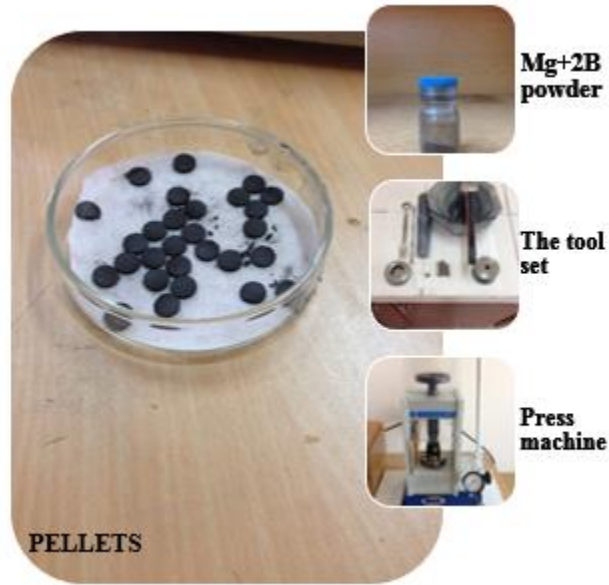


Figure 6.3. Mg+2B pellets and production units of hydraulic press and die.

Fe tubes used for PIT and PeIT methods were chosen to have outer / inner diameters of 12 / 9 mm, respectively. The Fe tubes were initially cleaned in acetone for 15 minutes using an ultrasonic cleaner (Transonic 460/H). The sealing process for iron tubes was completed by using aluminum foils as shown in Figure 6.4.

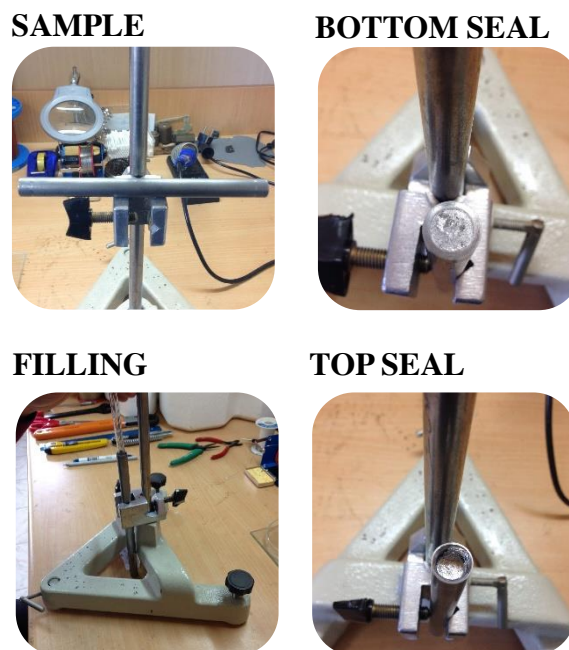


Figure 6.4. PIT or PeIT processed, sealed iron tube which is suitable for wire drawing.

6.3 Production of *in-situ* MgB₂/Fe Mono and Multi-filament Wires

In this study as-received iron tube without Mg coating was used to produce normal and excess-Mg wires while Mg-coated iron tube was only used for Mg-coated wire fabrication. The normal wires initially contain stoichiometric Mg+2B powder mixture with no additional magnesium. Excess-Mg wires have different amounts of additional Mg such that 1wt. % and 5wt. % Mg is initially mixed into the stoichiometric Mg+2B powder mixture. Mg-coated wires were made with stoichiometric initial powder mixture but a small amount of non-stoichiometry was introduced by Mg-coating process. Both PIT and PeIT methods are suitable to apply for the production of these wires. The composites, an example is shown in Figure 6.4, were cold-drawn from 12.0mm to 0.81mm outer diameter by using several circular dies. Two groove rolling machines were used in order to deform the fore point of the samples as represented in Figure 6.5. The intermediate heat treatments below the synthesis temperature of MgB₂ were applied between specific drawing steps to reduce the mechanical stress which was accumulated in the sheath material due to cold drawing. The multifilament wires with 18 superconducting filaments were made by inserting one copper stabilizer at the center of an iron tube and placing 18 mono core *in-situ* MgB₂ wires in the iron tube around copper stabilizer. The same wire-drawing procedure was followed for multifilament wire production.

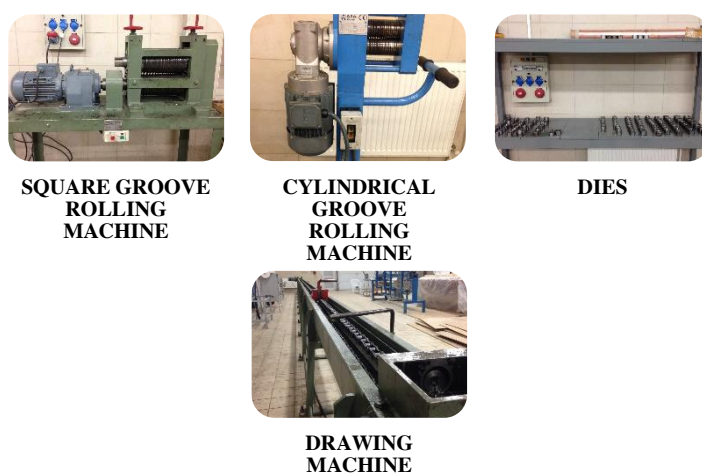


Figure 6.5. Dies with different internal diameters, two groove rolling machines and long wire drawing machine that are used for the production of wires.

6.4 Heat Treatments

Heat treatments were applied to MgB_2 wire samples at temperatures and times of 700°C -1h, 700°C -2h, 750°C -1h and 750°C -2h. The heat treatments were done under 5 bar argon atmosphere by using programmable tube furnace as shown in Figure 6.6. A stainless steel tube inside the cylindrical furnace was pre-cleaned by vacuum pumping and argon filling sequentially. After cleaning process, the furnace was set to synthesis temperature and in argon atmosphere with 5 bar pressure in order to prevent oxidation of the wire samples.



Figure 6.6. A programmable tube furnace with required installation parts.

In the present thesis, wire samples are classified according to the synthesis temperatures and production techniques as shown in Table 6.1. The stoichiometric $\text{Mg}+2\text{B}$ powder mixture is only called F5. The code *P* denotes the Pellet-in-tube method, the code *MG* is used for Mg-coated samples and the code *E* is for excess amount of Mg which is added to initial $\text{Mg}+2\text{B}$ powder in certain amounts of 1wt. % (*E1*) and 5wt. % (*E5*) of total $\text{Mg}+2\text{B}$ mixture.

Table 6.1. Table represents all samples in groups.

SAMPLE TYPES	CODE	HEAT TREATMENTS	FILLING METHOD	WIRE DIAMETER (mm)	SYMBOL	SAMPLE GROUP NUMBER
Normal wires	F5	700 °C-1h			A	1
	F5	700 °C-2h			B	
	F5	750 °C-1h	PIT	0.81	C	
	F5	750 °C-2h			D	
Mg coated wires	MGF5	700 °C-1h			A	2
	MGF5	700 °C-2h			B	
	MGF5	750 °C-1h	PIT	0.81	C	
	MGF5	750 °C-2h			D	
Mg coated wires	PMGF5	700 °C-1h			A	3
	PMGF5	700 °C-2h			B	
	PMGF5	750 °C-1h	PEIT	0.81	C	
	PMGF5	750 °C-2h			D	
Multifilament wires normal and Mg-coated	PMF5	700 °C-1h	PEIT	1.02	K	4
	PMGMF5	700 °C-1h			L	
Excess – Mg wires (1% 100-200 mesh Mg)	PE1F5	700 °C-1h			A	5
	PE1F5	700 °C-2h			B	
	PE1F5	750 °C-1h	PEIT	0.81	C	
	PE1F5	750 °C-2h			D	
Excess – Mg wires (5% 100-200 mesh Mg)	PE5F5	700 °C-1h			A	6
	PE5F5	700 °C-2h			B	
	PE5F5	750 °C-1h	PEIT	0.81	C	
	PE5F5	750 °C-2h			D	

6.5 The Structural Analysis Method

Structure and phase formation analysis of MgB₂ superconducting wires were performed by means of Rigaku MultiFlex diffractometer (CuK α radiation, $\lambda = 1.5418$ Å) in Figure 6.7. A superconducting core was extracted after the iron sheath was stripped off. This core was brought to powder form by grinding for XRD analysis which was carried out between the angles of $2\theta = 10^\circ$ and 90° with a $5^\circ/\text{min}$ scan speed (XRD beam acceleration, 38kV/28mA).



Figure 6.7. X-ray diffractometer for crystal structure analysis.

6.6 Surface Analysis

The scanning electron microscope (SEM) sends a focused beam of high energy electrons to the surface of solid samples. The signals generated from electron-sample interactions give information about the morphology, chemical composition, crystal structure and grain orientations of the sample. The surface morphology analysis of superconducting MgB₂/Fe wires was made by using a scanning electron microscope (JEOL 6390-LV) as shown in Figure 6.8. The SEM pictures were obtained from fracture or polished surfaces of the wire samples. The fracture surface was used to study core structure such as voids, micro cracks, etc. However a polished surface was needed in order to examine the grain structure and connectivity between the grains. The polishing method was done in stages by using sand papers which have different particle sizes and a polishing machine is shown in Figure 6.9. SEM images provided information about the microstructure and Energy Dispersive X-Ray Spectroscopy (EDS) was used to examine the phase formations in some special cases, especially for Mg-coated samples.

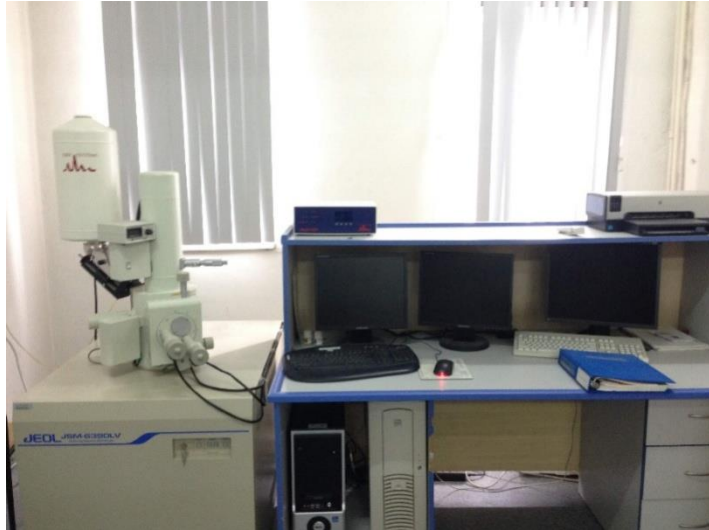


Figure 6.8. Scanning electron microscope device (JEOL 6390-LV).



Figure 6.9. The polishing machine is on the left and the mounting press is on the right.

6.7 Electrical Characterization Techniques

Electrical characterization of MgB_2/Fe wires were examined by using resistance-temperature (R - T) and current-voltage (I - V) measurements. These measurements were performed by using closed-cycle helium cryostat system as shown in Figure 6.10. The measurement system is capable of running 1A dc current at maximum and applying up to 7T magnetic field. The samples were placed in the cryostat system in perpendicular to the magnetic field, and the system was cooled in a zero magnetic field (ZFC). Four

probe contact method was used to measure temperature dependence of sample resistance for a 50mA dc current in a temperature region ranging from 20K to 50K. The critical current density (J_c) value was determined from the current-voltage measurements by using $1\mu\text{V}/\text{cm}$ criteria.



Figure 6.10. Electrical characterization measurement system.

7. RESULTS AND DISCUSSIONS

In this thesis, the *in-situ* processed normal, Mg-coated, and excess-Mg MgB₂/Fe superconducting wires were produced by using PIT and PeIT initial filling methods. Transport properties of each sample were investigated by means of resistivity-temperature (ρ - T) and in-field current-voltage (I - V) measurements. The crystal structure and surface morphology of the samples were analyzed by X-ray diffraction and scanning electron microscopy techniques, respectively. Residual resistivity ratios, critical current density, and n -values of the wire samples were calculated as functions of sintering time and temperatures.

7.1 Temperature Dependent Resistivity Measurements

The temperature dependent resistivity curves of the Mg-coated and normal wires in a zero magnetic field are given in Figures 7.1(a) and (b), respectively. The samples were heat treated at 700 and 750°C for 1 and 2 hours. The resistivity measurements of superconducting wires were performed on the round wires with outer diameters of 0.81mm by applying 50mA dc transport current. Figure 7.1(a) demonstrates that the superconducting phase transition for the Mg-coated samples is very sharp and the resistivity levels for these wires are below the 11 $\mu\Omega$.cm. The 2C-sample has the lowest resistivity around 6 $\mu\Omega$.cm. The resistivity values for Mg-coated samples are slightly lower than the resistivity of normal samples which is higher than 10 $\mu\Omega$.cm as seen in Figure 7.1(b). The changes in heat treatment conditions caused irregular changes in the resistivity of Mg-coated wires. This irregularity was not observed in normal samples and resistivity of the normal samples decreased with increasing sintering time and temperature. On the other hand, the superconducting transition for normal samples was found more dependent on heat treatment conditions and the transition width was generally broader than that of the Mg-coated wires.

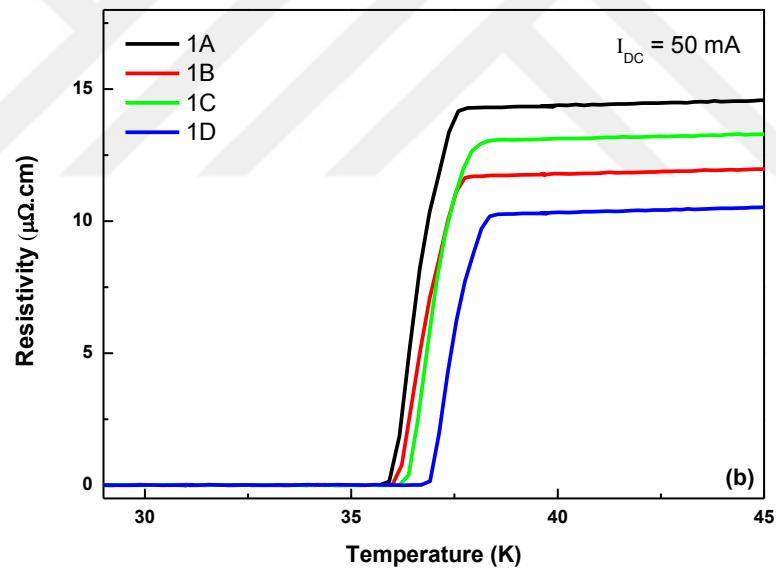
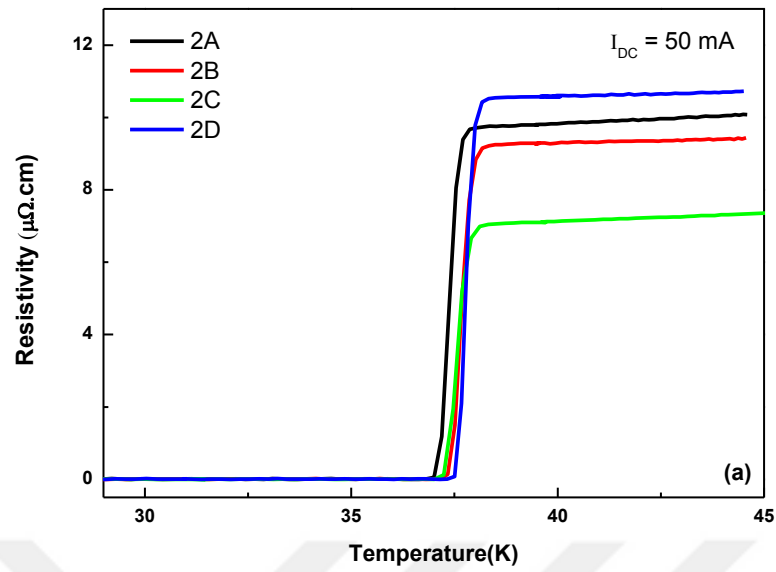


Figure 7.1. Temperature dependent resistivity ($\rho - T$) curves of (a) Mg-coated and (b) normal mono core MgB_2/Fe superconducting wires with OD = 0.81mm as functions of sintering time and temperature. (A: 700°C-1h, B: 700°C-2h, C: 750°C-1h, D: 750°C-2h)

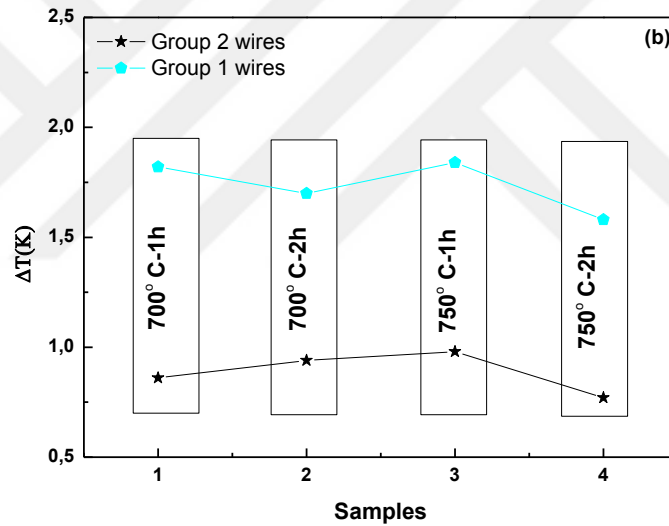
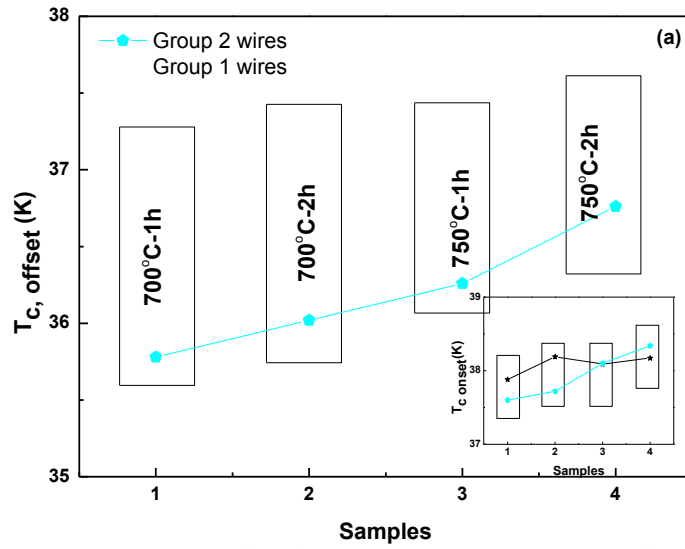


Figure 7.2. (a) The offset critical temperature ($T_{c,offset}$) and (b) superconducting phase transition width ($\Delta T = T_{c,offset} - T_{c,onset}$) values of Mg-coated and normal wires. The samples are coded as 1- 700°C, 1h, 2- 700°C, 2h, 3- 750°C, 1h, and 4- 750°C, 2h according to heat treatment time and temperature. The inset in Figure 7.2(a) represent the $T_{c,onset}$ values for the same samples.

A detailed analysis of offset and onset transition temperature values of Mg-coated and normal wire samples are given in Figure 7.2(a) and in the inset, respectively. $T_{c,onset}$ is the temperature at which the transition from the normal state to the superconducting state begins, while $T_{c,offset}$ is the temperature value at which the zero resistance is achieved. The superconducting transition width ($\Delta T = T_{c,onset} - T_{c,offset}$) was

found smaller than 1K for Mg-coated samples regardless of sintering conditions as shown in Figure 7.2(b). This is due to the fact that although the $T_{c,onset}$ values of normal and Mg-coated samples are close to each other, the $T_{c,offset}$ values of the Mg-coated wires are higher than the normal wires as shown from the inset in Figure 7.2(a). The sharp phase transition in Mg-coated samples indicates that the samples are of good crystallinity and homogeneity. The $T_{c,onset}$ and $T_{c,offset}$ values of normal sample slightly increased with increasing of the sintering time and temperatures but, the relative increase of $T_{c,onset}$ and $T_{c,offset}$ values also resulted in fluctuations at ΔT values as shown in Figures 7.2(a) and (b). The resistivity measurements revealed that the Mg-coated wires have a better transition to the superconducting phase than the normal wires under various sintering conditions.

Resistivity measurements were also carried out on different sample groups in order to determine the reproducibility, homogeneity and efficiency of Mg-coated samples. The homogeneity of the Mg-coated wire was demonstrated with wires reproduced again by using the PeIT method, and its efficiency was tested by comparing the transport characteristics of the wires containing excess Mg. The temperature dependent resistivity measurements of Mg-coated, 1wt. %, and 5wt. % excess Mg added wires were done in zero magnetic field by applying 50mA dc current. The results are given in Figures 7.3(a) to 7.3(c). The same heat treatment procedure was followed for all wires. In Figure 7.3(a), it is seen that the resistivity levels for Mg-coated wires are close to each other ranging between 10 and 12 $\mu\Omega$.cm. However, the resistivity values of 1wt. % and 5wt. % excess-Mg added wires vary between 4 and 10 $\mu\Omega$.cm depending on the heat treatment condition. Such a result is important in terms of the stability and reproducibility of the Mg coated wires. Although the samples with excess Mg have narrow normal-to-superconducting phase transition width, there is no shift in the $T_{c,offset}$ and $T_{c,onset}$ values of the Mg-coated wire samples that varies depending on the heat treatment condition as given in Figure 7.3(a). Mg-coated samples already have an excessive amount of Mg but this value is less than 1wt. % of total initial Mg+2B powder. Here it is remarkable to note that the resistivity level tends to decrease with increasing excess Mg ratio because the metallic phase is dominated within the sample. When the amount of excessive Mg inside the samples is considered, Mg-coated samples have the least amount of excess Mg among the non-stoichiometric wire samples, but they are

more stable than wire samples containing 1wt. % and 5wt. % excess-Mg under various sintering conditions and exhibit good superconducting transition properties as well.

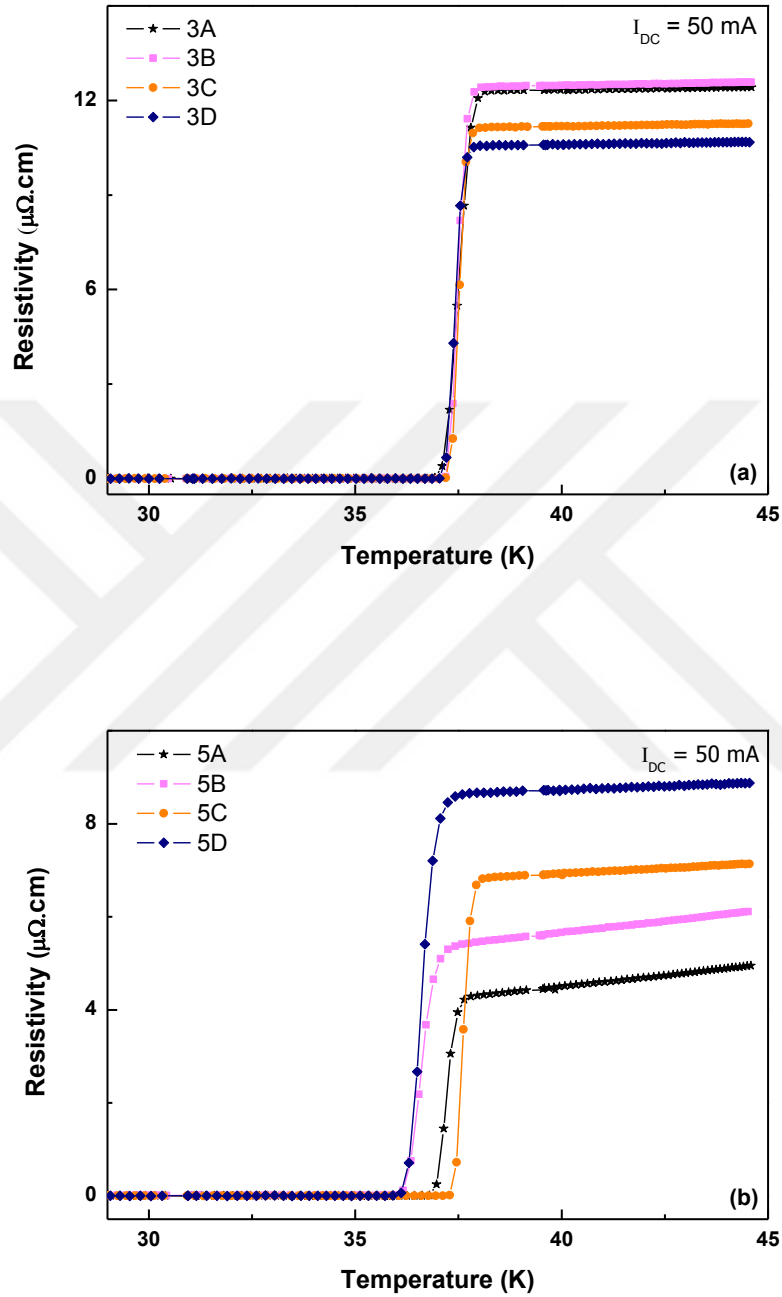


Figure 7.3. The resistivity versus temperature curves for (a) Mg-coated, (b) 1wt. % excess-Mg, and (c) 5wt. % excess-Mg mono core MgB₂/Fe wires with 0.81mm outer diameter (on the next page). The same heat treatment conditions were applied for all samples. Mg-coated wire has an excess-Mg which is less than 1wt. % of total Mg+2B. All the samples were produced by using the PeIT method. (A: 700°C-1h, B: 700°C-2h, C: 750°C-1h, D: 750°C-2h).

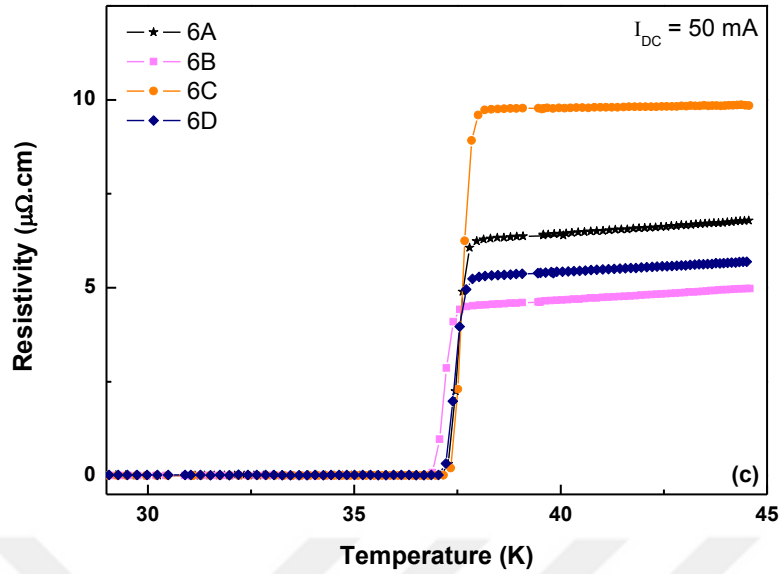


Figure 7.3. (cont'd) The resistivity versus temperature curves for (a) Mg-coated, (b) 1wt. % excess-Mg, and (c) 5wt. % excess-Mg mono core MgB_2/Fe wires with 0.81mm outer diameter. The same heat treatment conditions were applied for all samples. Mg-coated wire has an excess-Mg which is less than 1wt. % of total Mg+2B. All the samples were produced by using the PeIT method. (A: 700°C-1h, B: 700°C-2h, C: 750°C-1h, D: 750°C-2h).

The $T_{c,onset}$, $T_{c,offset}$, and ΔT values were also acquired from the resistivity measurements of Mg-coated, 1wt. %, and 5wt. % excess-Mg non-stoichiometric MgB_2/Fe wires as a function of heat treatment condition in Figures 7.4(a) to (c). Figure 7.4(a) shows that the $T_{c,offset}$ values of Mg-coated and 5wt. % excess-Mg wires are close to each other and do not change much with a heat treatment condition but 1wt. % excess-Mg wire exhibits an unstable $T_{c,offset}$ behavior when the sintering time and temperature is changed. This kind of variation is also relevant at $T_{c,onset}$ values of 1wt. % and 5wt. % excess-Mg samples. However, such a case was not observed at $T_{c,onset}$ values of Mg-coated sample as shown in Figure 7.4(b). Figure 7.4.(c) demonstrates that ΔT values obtained for the Mg-coated wires are around the 1K and completely below the 1K for 5wt. % excess-Mg samples. As a result, the superconducting phase transition for both Mg-coated and 5wt. % excess-Mg wires produced by the PeIT method is sharp and completed in a temperature range of 1K. The variations in ΔT values of 1wt. % excess Mg sample are indicative that a small amount of Mg cannot be distributed homogeneously by the mixing method.

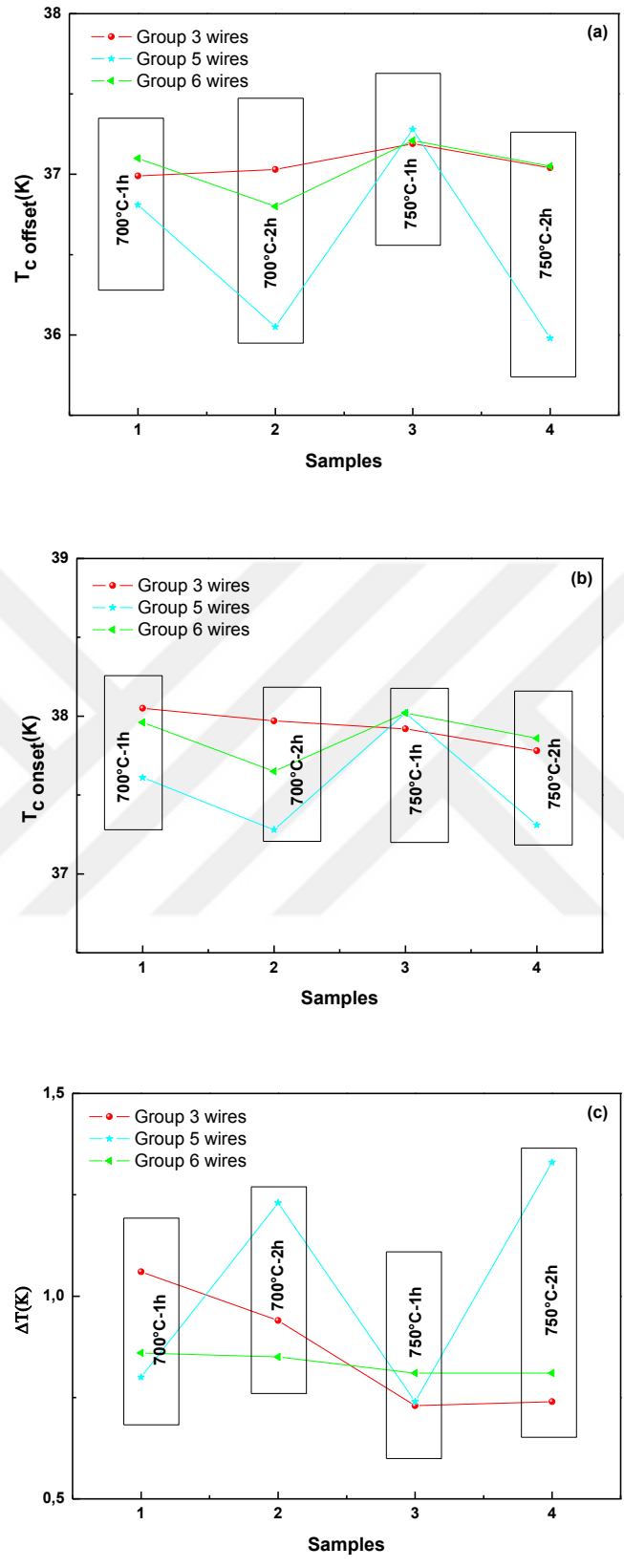


Figure 7.4. (a) $T_{c,offset}$, (b) $T_{c,onset}$, and (c) ΔT values for Mg-coated, 1wt. %, and 5wt. % excess Mg wires produced by PeIT method. The data is extracted from the ρ - T curves in Figure 7.3.

Figure 7.5 represents the temperature dependent resistivity measurements of the normal and Mg-coated MgB₂/Fe multi-filamentary wires performed under a zero magnetic field with a 50mA dc applied current. Heat treatments were carried out at 700°C for 1h on the wire samples with 1.02mm outer diameters. The superconducting transition width for both samples is about the 1.1K as shown in Table 7.1. $T_{c,offset}$ and $T_{c,onset}$ values of multi-filamentary wires were obtained relatively low in comparison to the mono core wire samples. It was found that that there was no noteworthy difference between the resistivity-temperature curves of normal and Mg-coated multi-filamentary wire samples. This result showed that a small amount of coated Mg lost its effect on thin superconducting filaments, but also proved that Mg-coating directly affected the transport properties of mono core wires.

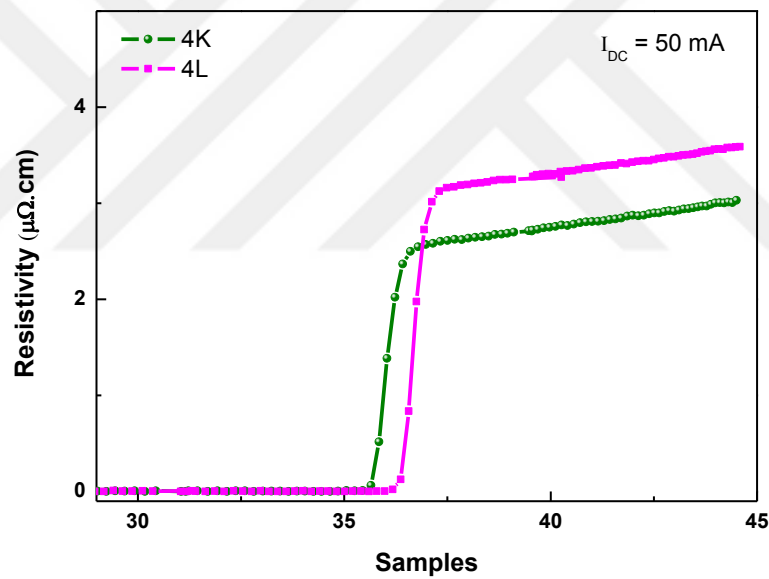


Figure 7.5. The temperature dependent resistivity curves of Mg-coated (L) and normal (K) multi-filamentary *in-situ* PIT processed MgB₂/Fe wires sintered at 700°C for 1h. The number of filaments in these wires is 18+1.

Table 7.1. $T_{c,offset}$, $T_{c,onset}$, and ΔT values for normal (K) and Mg-coated (L) MgB_2/Fe multifilamentary wires.

Samples	$T_{c,offset}$ (K)	$T_{c,onset}$ (K)	ΔT (K)	Sintering Temperature (°C)	Sintering Time (h)
4K	35.51	36.61	1.10	700	1
4L	36.17	37.28	1.11	700	1

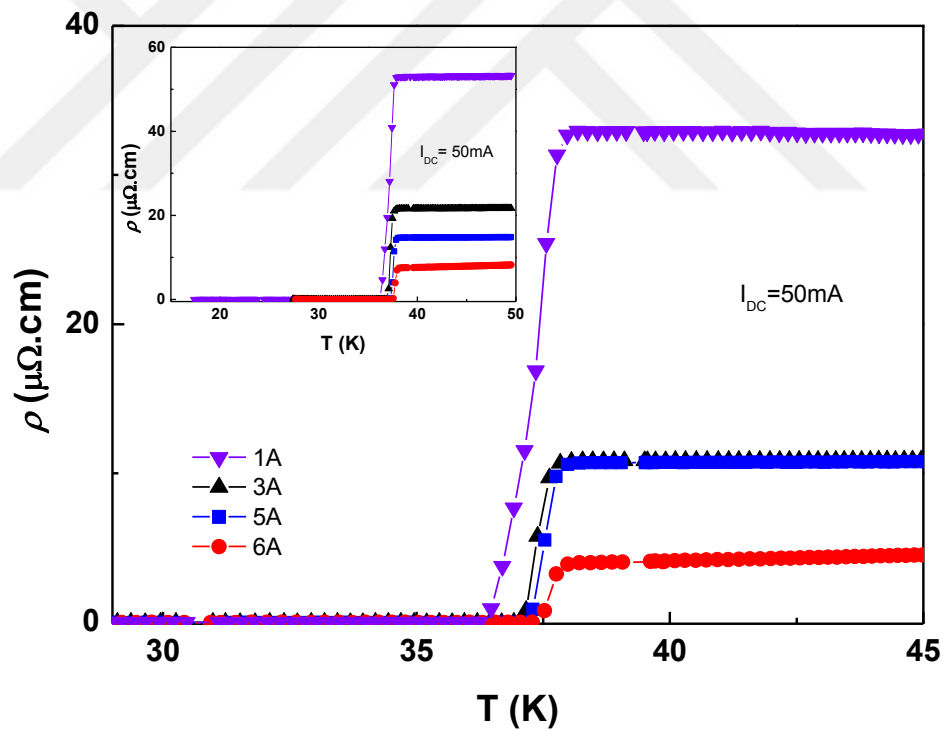


Figure 7.6. Temperature dependent resistivity values of MgB_2/Fe wire samples heat treated at 700°C for 1h. The sample codes: 1A- Normal, 3A- Mg-coated, 5A- 1wt. % excess-Mg and 6A- 5wt. % excess-Mg. The inset shows $\rho(T)$ characteristics of the same wires annealed at 750°C for 1h.

Figure 7.6 shows the comparative resistivity $\rho(T)$ curves which belong to MgB_2/Fe wire samples of normal (stoichiometric), <1 wt. % Mg-coated, 1 wt. % and 5 wt. % excess-Mg synthesized at 700 and 750°C for 1h in a comparative manner. The resistivity measurements were carried out on the stripped wire samples, and their superconducting core diameters were measured between 0.56mm and 0.58mm. A remarkable change is observed between the resistivity values of samples at 40K as a function of excessive amount of Mg in Figure 7.6. When the excessive Mg ratio was increased to 5wt. %, it was observed that the $\rho(40\text{K})$ values were lower. A difference about $30\mu\Omega\cdot\text{cm}$ or higher was reached in the resistivity level when a comparison was made between non-stoichiometric and normal (stoichiometric) samples as shown in the inset of Figure. 7.6. Also, the phase transition width values (ΔT) were found below the 1K for non-stoichiometric wires.

Some important parameters such as effective cross-sectional area fraction (A_F), residual resistivity ratio (RRR) values of wire samples were calculated, and these values are presented in Table 7.2. The A_F and RRR values were used to compare the wire samples heat treated at 700°C and 750°C for 1h in each sample group. The data required for the calculation of these parameters were obtained from the resistivity measurements of stripped mono core wires. Table 7.2 shows that the RRR values of the wire samples are progressively increasing in proportion to the increase in the amount of excess Mg content. The highest RRR value was obtained as 5.52 for the sample-6A. On the other hand, when the sample groups were examined separately, variations in RRR values with the heat treatment temperature and time do not follow a meaningful regular pattern as the amount of excess Mg content changes. A significant difference was observed between RRR values of sample-6A and sample-6C but no significant difference was observed in Mg-coated samples. Contrary to RRR values, the A_F values of the samples do not exhibit a regular association in relation to the fabrication parameters, and the highest A_F value was calculated to be 0.36 for sample-5A. (Rowell, 2003). When a comparison was made between the normal and non-stoichiometric Mg samples, a relatively higher A_F values for the excessive Mg samples than that of the normal sample were obtained regardless the sintering temperature. In general, a high A_F value denotes the existence of a good connectivity between the grains. The results in Table 7.2 showed that the excess Mg addition up to 5wt. % promoted the grain connectivity of the MgB_2 wire samples. Dependence of A_F value on sintering conditions is much weaker when a

small amount of excess-Mg was incorporated by Mg-coating method, as a result very similar A_F values are maintained.

Table 7.2. The RRR and A_F values of the MgB_2/Fe wire samples heat treated at 700 and 750 °C for 1h. $\Delta\rho_{ideal} = 7.3 \mu\Omega.cm$ (Chen et al., 2008). MgB_2 core diameters are 0.56mm for Mg-coated - normal wire samples and 0.58mm for 1wt. % - 5wt. % excess-Mg samples.

Wire samples	RRR (ρ_{300K}/ρ_{40K})	$\Delta\rho(\mu\Omega.cm)$ ($\rho_{300K}-\rho_{40K}$)	A_F $\Delta\rho_{ideal} / \Delta\rho$	$T_{c,onset}$ (K)	$T_{c,offset}$ (K)	ΔT (K) ($T_{c,onset} - T_{c,offset}$)
1A	2.14	34.0	0.21	37.8	36.2	1.6
1C	2.13	59.9	0.12	37.6	36.0	1.6
3A	2.17	24.4	0.30	37.6	36.9	0.7
3C	2.17	25.4	0.29	37.5	36.9	0.6
5A	2.31	20.1	0.36	37.7	37.1	0.6
5C	2.48	21.7	0.34	37.7	37.3	0.4
6A	5.52	25.2	0.29	37.8	37.3	0.5
6C	3.79	21.2	0.34	37.9	37.6	0.3

7.2 Current-Voltage Measurements

The current-voltage measurements were carried out under external magnetic field ranging between 0 to 7T at temperatures below the T_c by using a closed-cycle cryostat system. Transport current was applied up to 1A at maximum, not any higher, in order not to cause Joule heating on the wire samples. The engineering critical current density (J_{ce}) values of the wires were determined by using $1\mu V/cm$ criteria. $I-V$ measurements were done on the wire samples which were sintered at different heat treatment conditions such as 700-750°C for 1 and 2h. The four probe method was carried out on the wires that were cut to 25mm length and a perpendicular magnetic field ($\vec{B} \perp \vec{I}$) was applied during measurements.

Figures 7.7(a) and (b) show the $E-J_e$ behaviors of Mg-coated and normal wire samples under different external magnetic fields at $T = 28K$. J_e is the engineering current density and calculated over total wire diameter. A significant difference between the transport properties of normal and Mg-coated MgB_2/Fe superconducting wires was observed for the same operating temperature value. Although the $E-J_e$ characteristics of the wires were close each other, the external magnetic field value applied to normal

samples was 2.5T lower than the field value applied to the Mg-coated wires as shown in Figures 7.7 (a) and 7.7 (b). The highest J_{ce} ($T=28K$) among the Mg-coated wires was obtained for sample-2A as above the $10^2 A/cm^2$ under $B = 6.75T$. The $J_{ce} = 10^2 A/cm^2$ level could not be reached in normal wires, even at a lower magnetic field of $B = 4.5T$. It was revealed that Mg-coating method improved the transport properties of MgB_2 mono core wires.

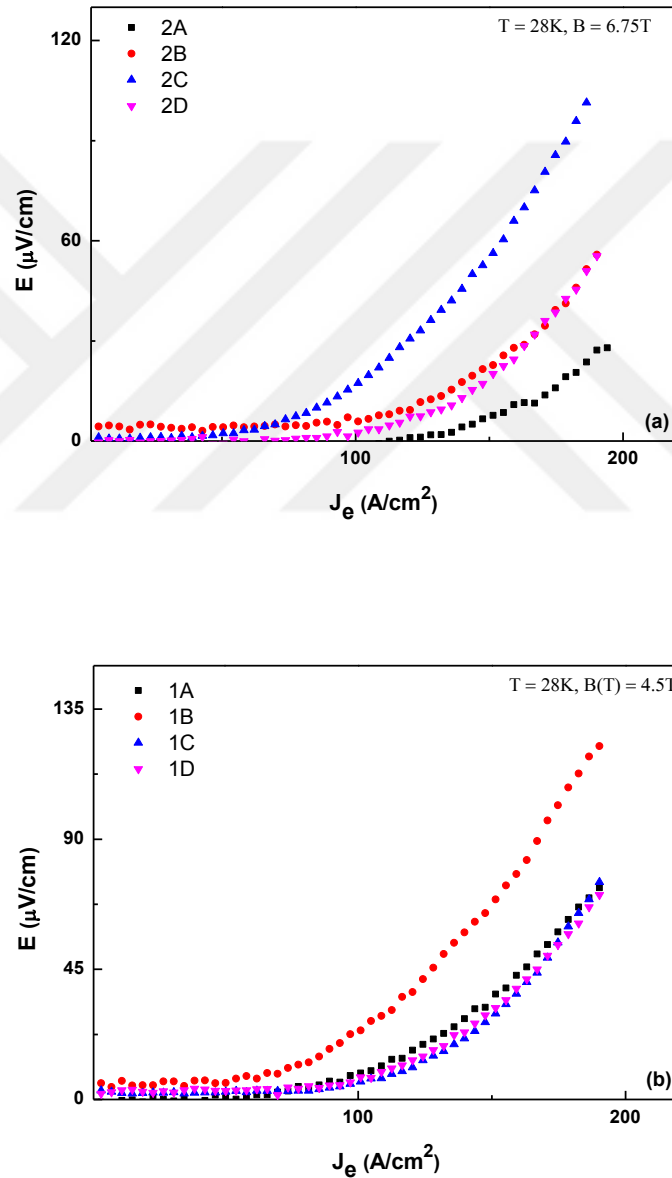


Figure 7.7. The E vs. J_e curves obtained for (a) Mg-coated and (b) normal superconducting wires at various sintering time and temperatures. The total wire diameter is 0.81mm and both samples were produced by using PIT method.

The current-voltage measurements were also performed on MgB₂/Fe superconducting wires having 1wt. and 5wt. % excess-Mg at the same operating temperature of 28K and under the external magnetic field of 6.75T as shown in Figures 7.8(a) and (b). It was found that excess amount of Mg improved well the transport properties of MgB₂ wires for all heat treatment conditions in comparison to the results obtained for normal samples given in Figure 7.8(b). On the other hand, the high J_e 's of Mg-coated samples in Figure 7.8(c) could not be reached, even in samples with 5wt. % excess-Mg which had higher J_{ce} values than the samples with 1wt. % excess-Mg. In accordance with the literature, the excess amount of Mg improved the transport properties of MgB₂ up to 5wt. %. However, the change in heat treatment conditions caused the variations on transport properties with increasing the amount of excess Mg. The electric field strength in Mg-coated samples is below the 30 μ V/cm even at J_e values as high as 2×10^2 A/cm² regardless of sintering time and temperatures. Under the same magnetic field value of 6.75T, electric field strength inside the 1wt. % and 5wt. % excess-Mg samples exceeded 150 μ V/cm level. The Mg coating method allowed for more stable and better transport properties under the external magnetic fields.

The E - J_e curves obtained for the Mg-coated wires produced by using PIT and PeIT initial filling methods are shown in Figures 7.7(a) and 7.8(c), respectively. It was revealed that increasing initial filling density with PeIT method also contributed to the transport properties of Mg-coated wires. The PeIT method contributed to the production of Mg-coated MgB₂ wires, which were less affected by changes in heat treatment time and temperature, acting more stable under the magnetic field. The electric field E was decreased from 100 μ V/cm to a level below 30 μ V/cm by PeIT method. The J_{ce} value was increased to 1.99×10^2 A/cm² for the Mg-coated wire sample under $B=7$ T. 1 wt. % and 5 wt. % excess-Mg samples were also produced by the PeIT method. The electric field strength in these samples increased very rapidly after the current density run through the wire sample exceeds its J_{ce} value. Such an enhancement in the electric field of superconducting wire samples with a low J_{ce} is not desirable because the stability and quench protection are the key issues in terms of superconducting magnet applications.

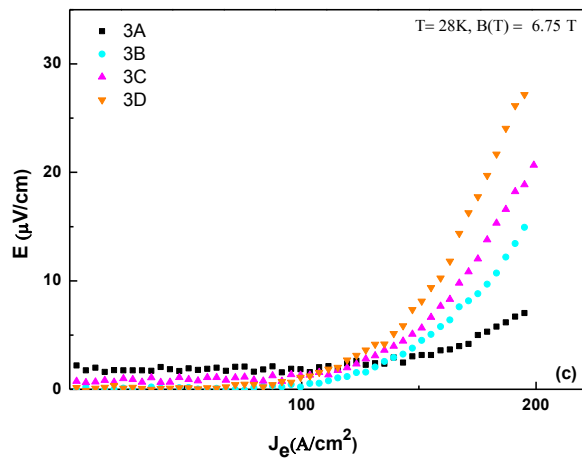
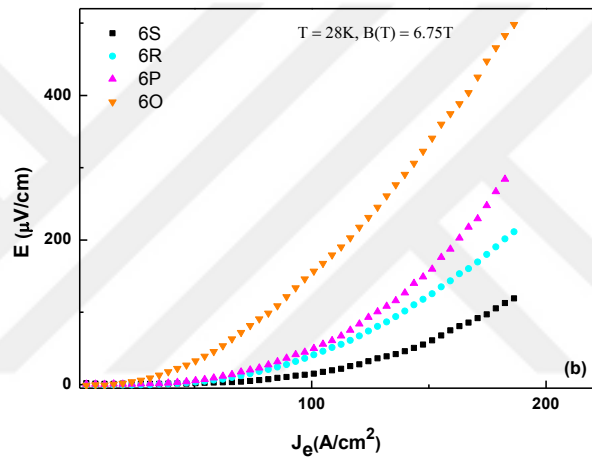
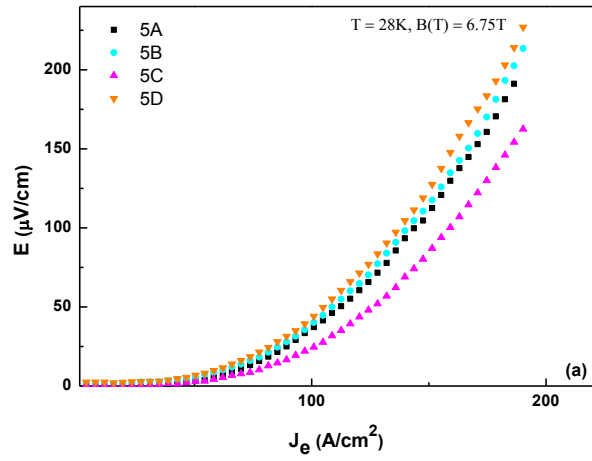


Figure 7.8. E vs. J_e characteristics for (a) 1wt. % excess-Mg, (b) 5wt. % excess-Mg, and (c) less than 1wt. % Mg-coated wire samples, respectively. All samples were fabricated by using the PeIT method.

J_{ce} values as a function of external magnetic field at 28K are given for all Fe/MgB₂ wire samples in Figure 7.9. The J_{ce} - B curves were drawn by taking into account the sintering temperature/time, and excessive amount of Mg. Excess Mg addition generally increased the J_{ce} under applied magnetic field as shown in Fig. 7.9. This was evidently shown that the highest J_{ce} level at $B = 7T$ and $T = 28K$ was achieved for the Mg-coated wire samples, despite they had the lowest initial excess-Mg among the non-stoichiometric wire samples. The results display that the Mg-coating method is not only an alternative method of excess Mg addition but also a powerful method which improves the transport properties of MgB₂ wires. A lower processing temperature and time (700°C, 1h) is preferable to increase $J_{ce}(B)$ of the Mg-coated MgB₂/Fe wires as shown in Figure 7.9. On the other hand, increasing the excess Mg ratio promoted the crystallinity in 1wt. % and 5wt. % excess-Mg samples which was verified by the increase in RRR values given in Table 7.2 but also, the increase in $J_{ce}(B)$ for 1wt. % and 5wt. % excess-Mg samples showed a tendency to saturation under low applied magnetic fields as seen in Fig. 7.9. This is a sign that more metallic phase was formed during the reaction by further increasing the initial excess Mg inside the sample. Changes in heat treatment conditions did not adversely affect the grain formation of Mg-coated wire samples.

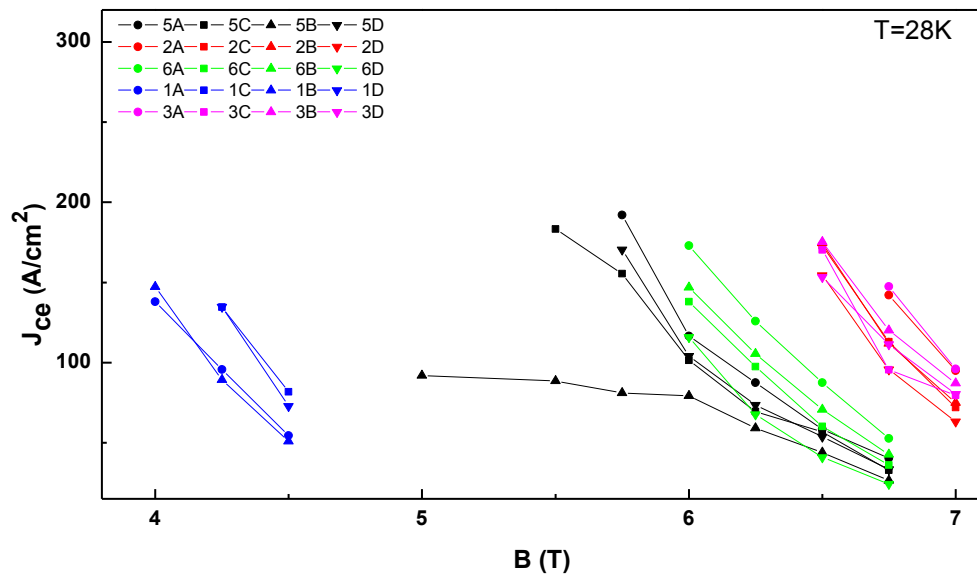


Figure 7.9. $J_{ce} - B$ curves at $T = 28K$ obtained for all sample groups. The engineering critical current density values were determined with $1\mu V/cm$ criteria.

Figure 7.10 represents n -values as a function of external magnetic field for all MgB₂/Fe wire samples at $T = 28\text{K}$. The n -values were calculated by fitting the E vs. J curves to a power-law relation, $E \sim (J)^n$. In a magnet design running in a permanent mode, the MgB₂ conductor must have a high n -value as possible. The n -value is a quantity dependent on temperature and magnetic field, and the range of $n = 10\text{-}20$ at 20K is acceptable for low-field applications of MgB₂ wires. In Figure 7.10, it is obvious that there is a significant difference between n -values of normal and excess-Mg wire samples. The n -value reached to 4.8 at $T = 28\text{K}$ and $B = 7\text{T}$ for the Mg-coated wire sample sintered at 700°C for 1h. Also when a comparison was made between the sample groups 2 and 3, some differences were observed in between n -values which belong to the Mg-coated samples that were produced by using PIT and PeIT methods. Whereas these differences showed that higher initial filling density is effective for improving the transport properties (Karaboga et al., 2017)

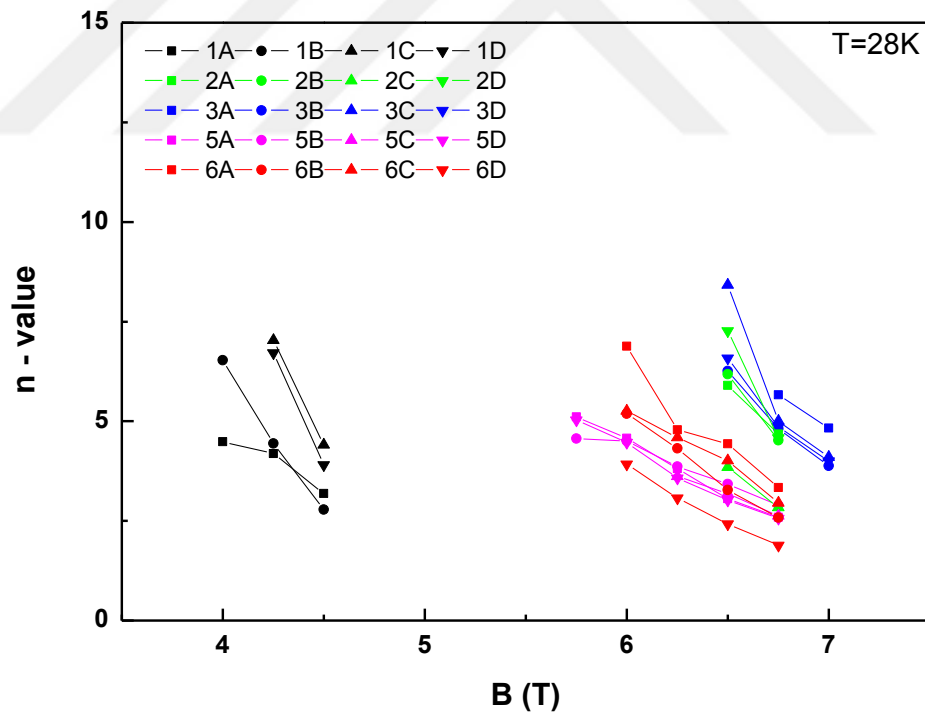


Figure 7.10. The n -values calculated for normal, Mg-coated, and 1wt. % excess-Mg and 5wt. % excess-Mg MgB₂ superconducting wire samples.

J_{ce} - B performance of Mg-coated wires were also measured at high applied currents up to 150A in liquid helium (4.2K) under external magnetic fields which range from 5T to 8T, results of these measurements are shown in Fig. 7.11. A high J_{ce} (4.2K) $> 10^4$ A/cm² was achieved under $B = 5$ T for all Mg-coated wire samples. The use of Mg-coated wire samples in low and medium magnetic field applications seems to be feasible.

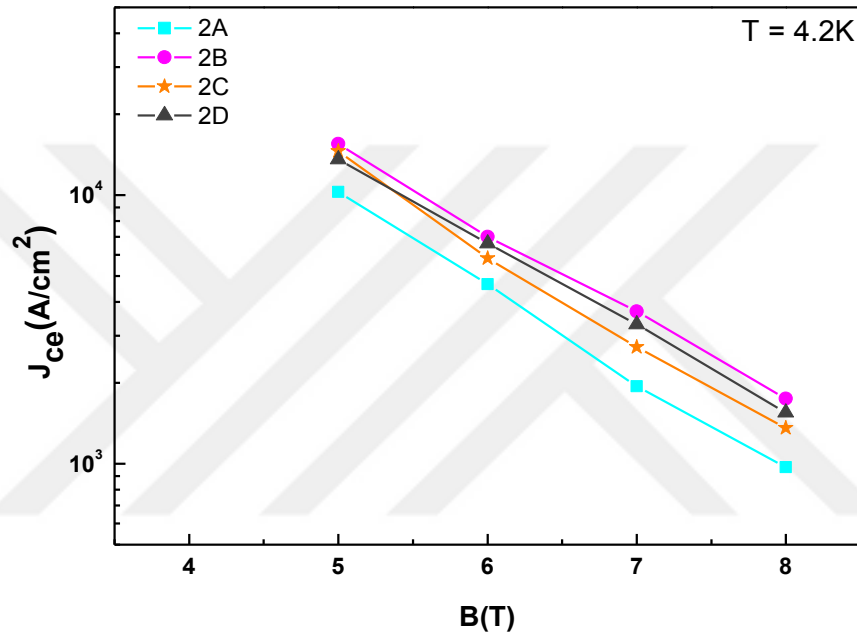


Figure 7.11. J_{ce} - B curves of four PIT processed Mg-coated MgB₂/Fe wire samples measured in liquid helium environment.

The E vs. J_e curves of normal and Mg-coated MgB₂/Fe multi-filamentary superconducting wires were also obtained in the presence of external magnetic field of 5T at $T = 28$ K as shown in Figure 7.12. The effect of Mg-coating process on transport properties of 18+1 multi-filamentary MgB₂/Fe wires was investigated. The results presented in Figure 7.12 show that the use of magnesium coated iron tube at minimum doubles the J_{ce} value of MgB₂/Fe wire from 22.1A/cm² and 46.3A/cm². This result is very promising for future Mg-coating studies. The properties of the MgB₂ multi-filamentary wire can be further improved by adjusting production parameters such as Mg-coating thickness, heat treatment time, and sintering temperature. Current discussions on Mg non-stoichiometry are also due to the discrepancies in processing

conditions. In this thesis, a new technique called internal Mg-coating was attempted to contribute to the issues on Mg non-stoichiometry. It was found that a small excessive amount of Mg significantly changed the transport properties of MgB₂/Fe wires such as J_{ce} and n -values under medium magnetic fields.

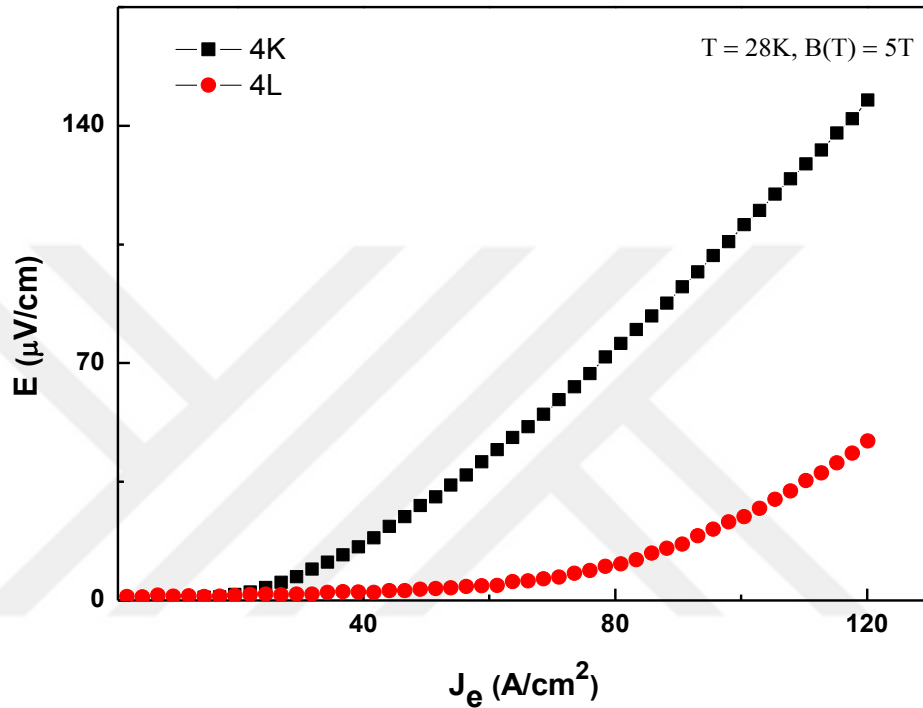


Figure 7.12. E vs. J_e curves of Mg-coated and normal *in-situ* MgB₂/Fe multi-filamentary wires.

7.3 XRD Measurements

The phase formation analysis of normal and Mg-coated wire samples was performed by means of x-ray diffraction measurements. Fe sheath was removed from the superconducting core before XRD measurements. A thin MgB₂ cylindrical core with a diameter of about 0.6mm was obtained after stripping off the Fe sheath. A small amount of powder obtained from the grinding of these thin cores was used in the XRD analysis. The Ag peaks which appear in the XRD patterns in Figures 7.13(a) and (b) arise from the silver holder which was used to spread the MgB₂ powder onto it because a small amount of MgB₂ powder could not cover the entire holder surface.

Figures 7.13(a) and (b) represent the XRD patterns of normal and Mg-coated samples, respectively. Difficulties in removing the Fe sheath caused different amounts of MgB_2 powder to be used in XRD analysis. This led to unintentional disproportion between the XRD peak intensities for different samples. As seen in Figures 7.13(a) and (b), peak intensities were relatively high for normal samples in comparison to that of the Mg-coated samples due to differences in the amount of powder used for XRD measurements. However, when the XRD patterns were examined for both samples, it was found that the amounts of impurity phases of un-reacted Mg and MgO were very similar and there was no significant difference between structural parameters of the samples. These results are not surprising, because the excess amount of Mg introduced into the structure was very low (less than 1wt. % of total Mg+2B). Presence of MgO phase may have resulted from the oxidation of Mg atoms in the starting precursor powders in air (Kim et al., 2007). The intensities for the un-reacted magnesium particles were also quite low for both samples. It is known that the Fe_2B phase starts to form at sintering temperatures above 575°C and its thickness depends on both heat treatment time and temperature (Grivel et al., 2006). Therefore, the Fe_2B formation was observed more or less in the XRD patterns of the normal and Mg-coated samples and more pronounced in relatively long time sintering such as 700°C and 750°C for 2h. Detection of Fe_2B peaks in the XRD patterns of Mg coated samples indicate that Mg coating method is not sufficient to prevent Fe_2B formation at core/sheath interface region completely.

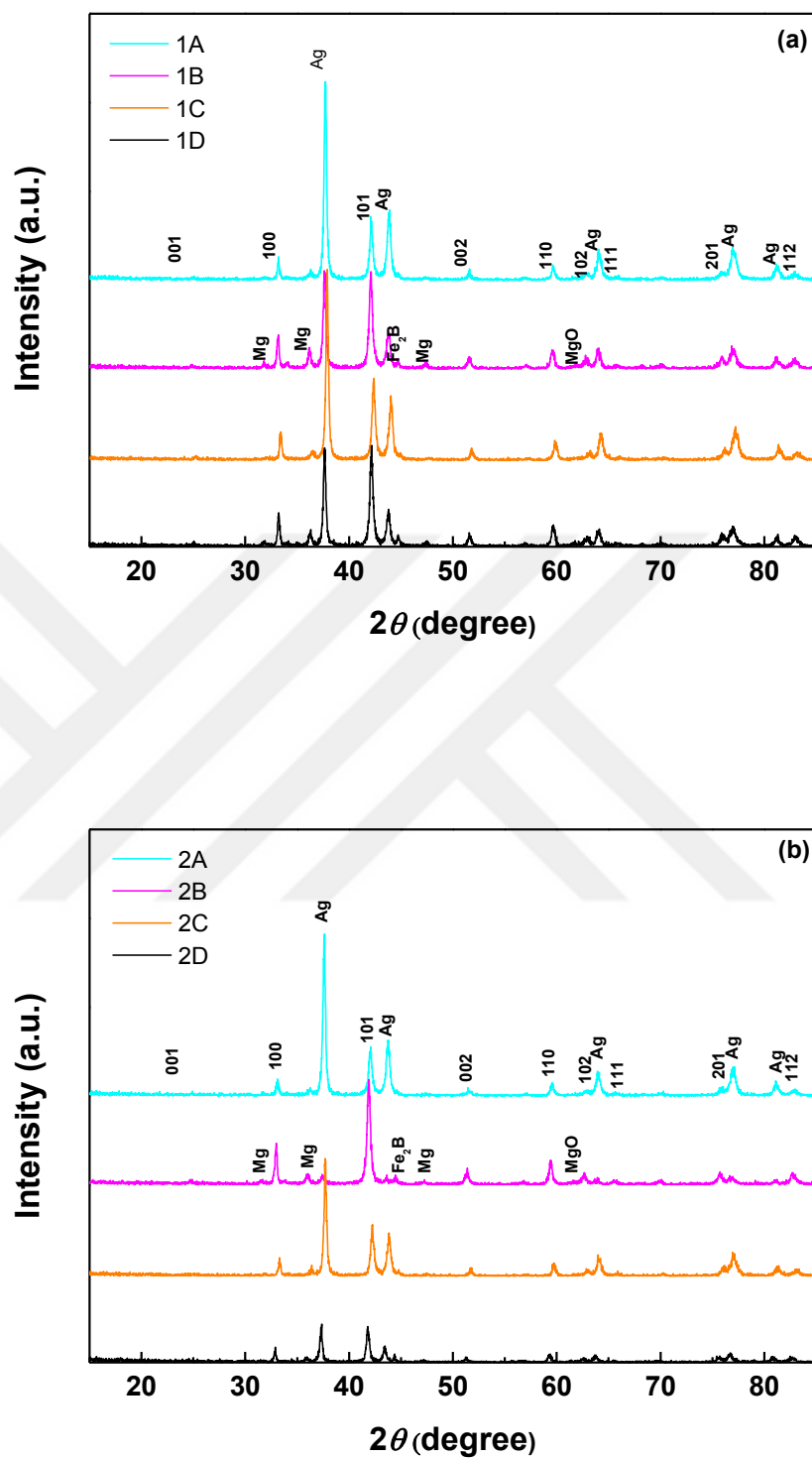


Figure 7.13. XRD patterns of (a) normal and (b) Mg-coated wires produced by using PIT initial filling method.

XRD patterns were also obtained for the PeIT processed normal, Mg-coated (additional Mg is less than 1wt. %), 1wt. and 5wt. % excess-Mg wire samples. Figures

7.14(a) and (b) show the x-ray diffraction peaks of the wire samples heat treated at 700°C and 750°C for 1h, respectively. X-ray diffraction analysis was performed only on these samples because their transport properties were better than the wire samples heat treated at the same sintering temperatures for 2h as shown in Figure 7.9. The un-reacted Mg peaks which appear between the 2θ angles of 30°C and 40°C in XRD patterns for the sample-5A and sample-6A were found to be more visible in comparison to that of the sample-5C and sample-6C. This result indicated that excess amount of Mg (especially for 5wt. %) was not sufficiently consumed to form more MgB_2 phase during 700°C for 1h sintering. The un-reacted Mg peak intensities were relatively low in the XRD patterns of normal and Mg-coated wire samples. Mg peak was quite low at 700°C and almost completely invisible at 750°C for Mg-coated samples. The Fe_2B phase formation also occurred in 1wt. % and 5wt. % excess-Mg samples and Fe_2B peak appeared in the vicinity of MgB_2 's main peak. Obtaining a relatively low Fe_2B peak for the Mg-coated sample suggested that the combination of Mg-coating and PeIT methods may be effective in inhibiting Fe_2B phase formation. XRD analysis showed that un-reacted Mg could be highly consumed by increasing the sintering temperature or sintering time in the excess-Mg samples, but the Fe_2B phase would also increase.

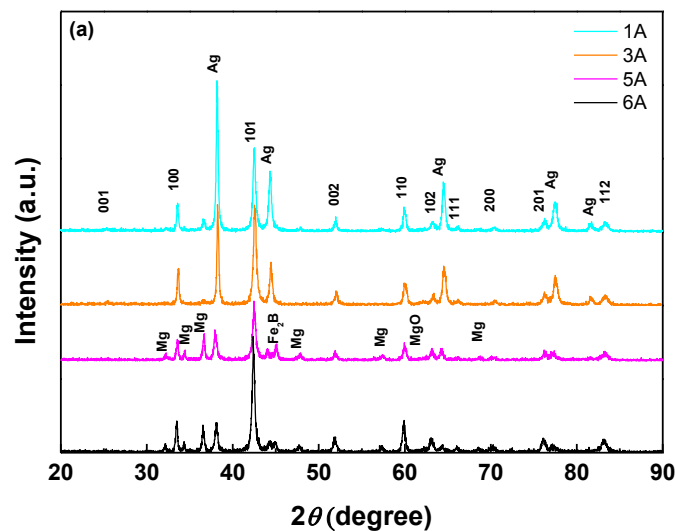


Figure 7.14. XRD patterns of all samples that are heat treated at (a) 700°C and (b) 750°C for 1h, respectively.

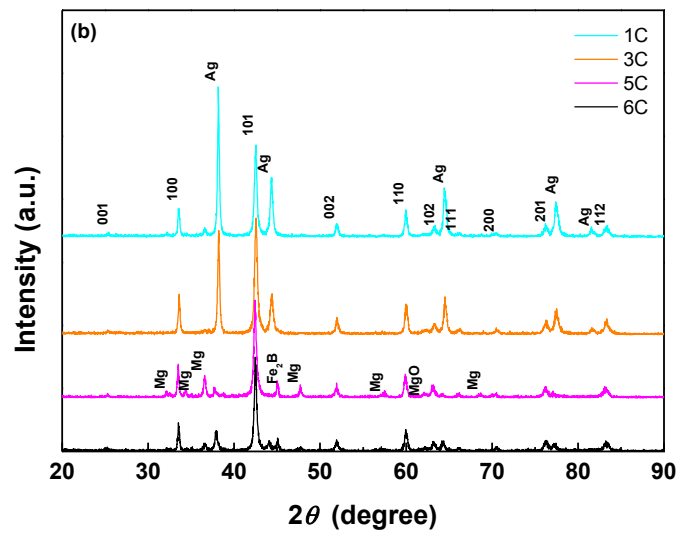


Figure 7.14. (cont'd) XRD patterns of all samples that are heat treated at (a) 700°C and (b) 750°C for 1h, respectively.

7.4 Scanning Electron Microscope (SEM) Analysis

The amount of excess Mg used for the internal coating process initially was determined to match about 10 wt. % of the total mass of stoichiometric Mg + 2B precursor powder. During the hot Mg coating process; the magnesium powder was allowed to evaporate, so a significant amount of magnesium powder was lost and only < 1wt. % Mg was coated on the inner walls of the iron tube. The hot Mg-coating method yielded Mg losses but, a thin and homogeneous inner Mg layer was obtained on the internal walls of Fe tube. Because the Mg layer was very thin, it was not possible to determine the thickness from the inner surface of the coated Fe tube. Therefore, elemental mapping was used to reveal that magnesium was coated on the inner surface of Fe tube as shown in Figure 7.15.

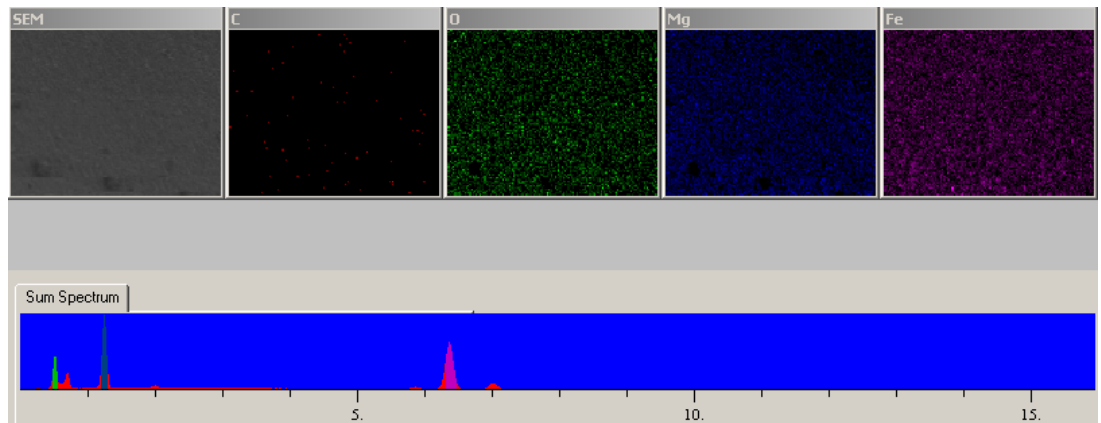


Figure 7.15. This image shows the elemental map analysis of a piece from Mg-coated Fe tube. Different colors represent the elements as follows: Red (carbon), green (oxygen), blue (magnesium), and pink (iron).

Figure 7.16 represents cross-sectional surface images which belong to the normal (Figs. 7.16(b)-(d)) and Mg-coated samples (Figs. 7.16(a)-(c)) taken from their fracture surfaces by using the SEM device. Deformations on the surface of the sheath material and core regions are due to fracturing. A thicker Fe wall which is observed clearly in the Mg-coated samples than the normal samples resulted from initial powder filling process. The Mg layer coated on the inner walls of the Fe tube can easily be damaged mechanically during filling processes. In order not to damage Mg layer which was already very thin, initial powder filling in PIT process was gentler. Therefore the initial filling density of Mg-coated samples was lower than that of the normal samples. As a consequence, a relatively smaller final core diameter was obtained. A high initial filling density is beneficial in order to reduce Fe₂B formation and to achieve better transport properties. Thus, PeIT method was found as a good candidate to achieve this goal.

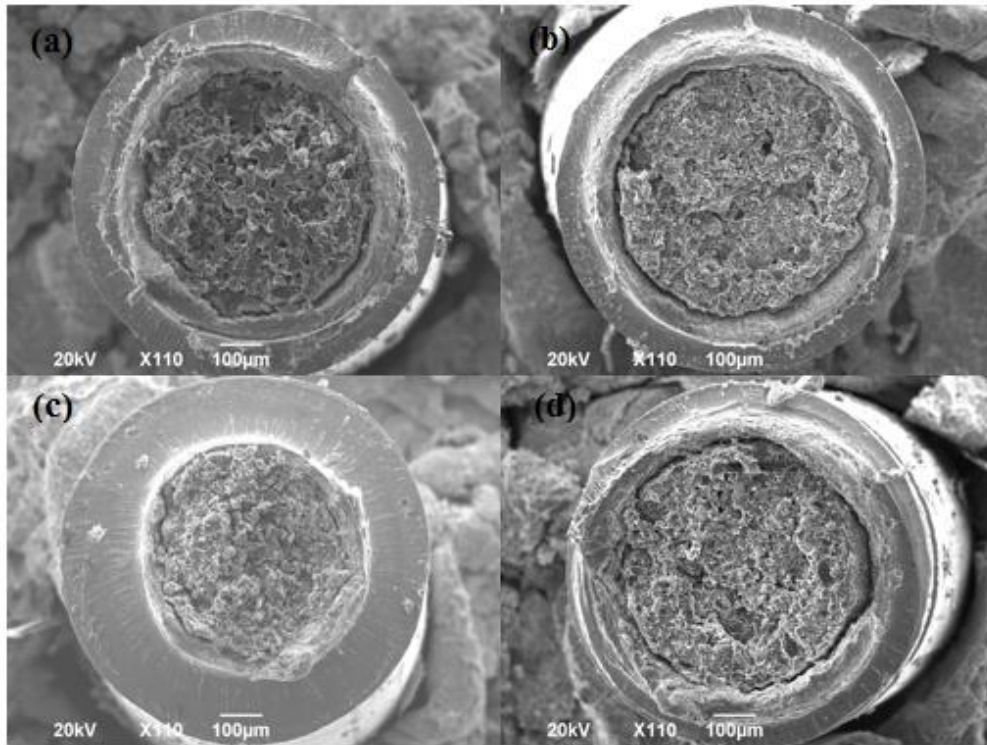


Figure 7.16. This figure shows the fracture cross sections of normal and Mg-coated samples. (a) and (c) Mg-coated samples synthesized at temperatures of 700°C and 750°C for 2h, respectively. (b) and (d) Normal samples synthesized at $T = 700^{\circ}\text{C}$ and 750°C for 2h, respectively. These samples were produced by using PIT method.

In Figure 7.17, the SEM images show some details about the surface morphology and grain structures that belong to the normal and Mg coated samples at two different magnifications. When the SEM images of Mg-coated samples in Figures 7.17(a) and (c) are examined in terms of granular structure, it is seen that Mg-coated samples have a denser structure and larger holes than that of the normal samples represented in Figures 7.17(b) and (d). The granular structures of the normal samples have a more porous appearance, as well as, more irregular stacks of volumes in comparison to Mg-coated samples. In Figures 7.17(e) and (g), it is observed that there are tight and small sized grain structures in Mg-coated samples according to the normal samples (Figs. 7.17(f) and (h)). These results suggested that the inclusion of excess Mg into the core structure by evaporation method promoted the formation of well-connected small grains. A small amount of excessive Mg was reacted more effectively with boron during synthesise in Mg-coated samples.

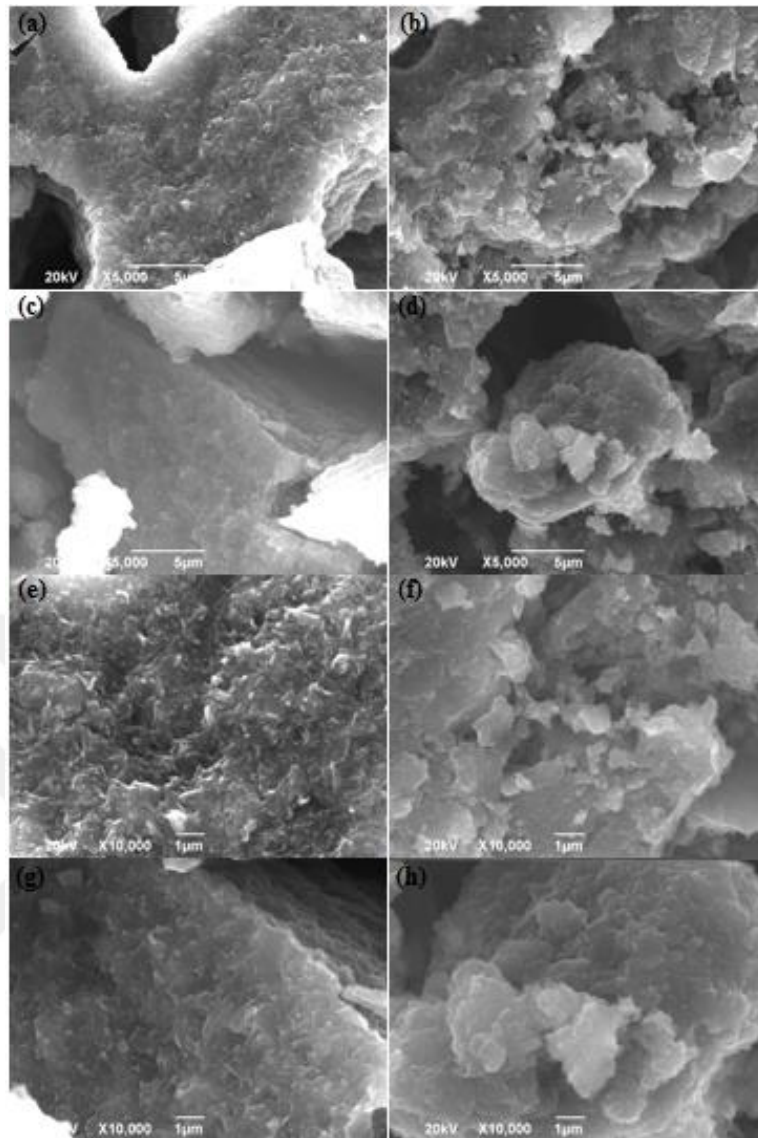


Figure 7.17. SEM images of PIT normal samples are seen on the right (b, d, f, h) and PIT Mg-coated samples are seen on the left (a, c, e, g). Top 2 rows are at x5000 magnification and bottom 2 rows are at x10000 magnification. Micrographs in the first and third rows were taken from the wires synthesized at 700°C and others were taken from the wires synthesized at 750°C, for 2h.

Microstructural analysis was also performed on the lateral surface, which is the area of all sides of the wires, excluding the area of its ends, of normal, <1 wt. % Mg-coated, and 5 wt. % excess-Mg stripped wires to reveal structural differences affecting the development of higher J_{ce} (and J_c) in Mg-coated samples. The SEM micrographs taken from core/sheath interface region at 20000 \times magnification are given in Figs. 7.18(a) to (c). Secondary electron micrographs originating from the near-surface regions of three types of wires have a different appearance in the interface region. Figure 7.18(b) shows that the Mg-coated sample contains long grains that resemble bars at the surface

and small grains close to each other beneath the surface. As seen in Figure 7.18(c), the grain structure of the sample containing 5wt. % excess-Mg is slightly different, where the structural differences between the layers are not as obvious as in the Mg-coated sample

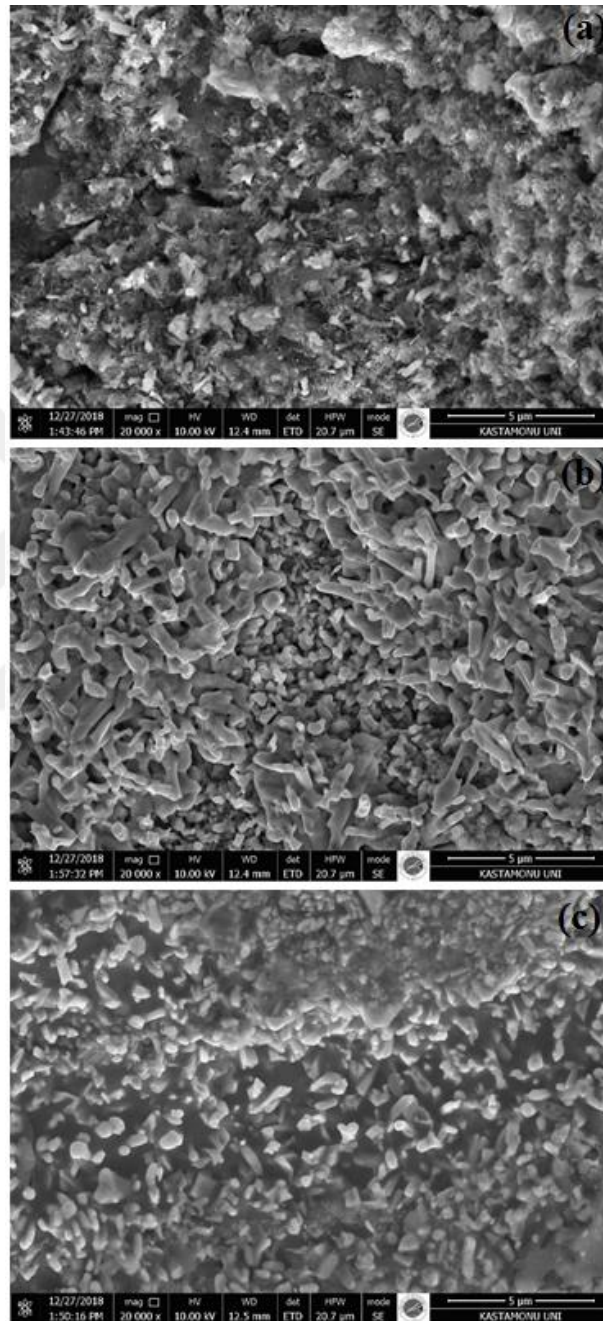


Figure 7.18. Microstructures of PeIT processed (a) normal (stoichiometric) MgB₂ wire synthesized at 750°C for 1h, (b) < 1wt. % Mg-coated wire synthesized at 700°C for 1h, and (c) 5wt. % excess-Mg wire synthesized at 700°C for 1h. These images obtained from the lateral surface of stripped wires with magnification of 20000×.

Energy dispersive x-ray spectroscopy was carried out on selected points at the lateral surface of the Mg-coated core to reveal the elements contained in the grains of different layers as shown in Figure 7.19.

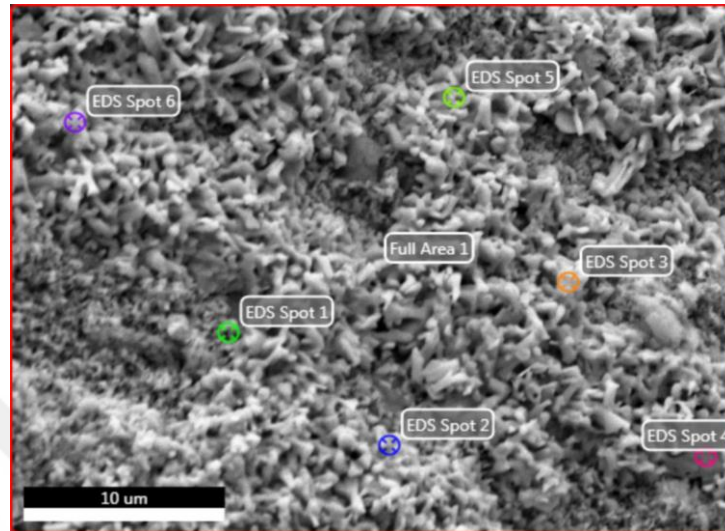
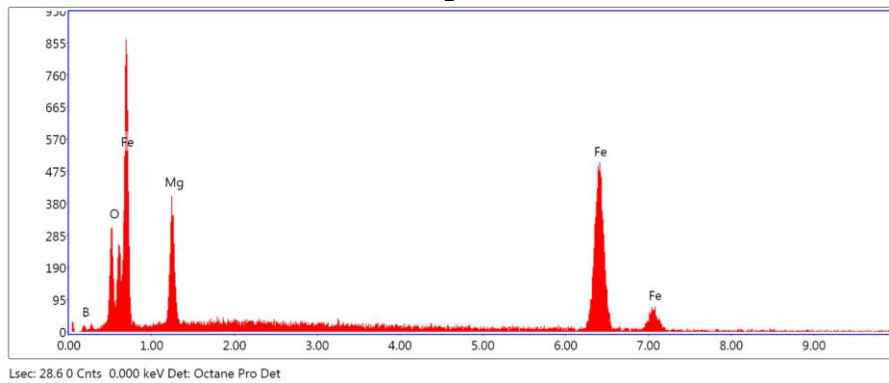


Figure 7.19. Spot EDS analysis of Mg-coated wire taken from different surface regions.

EDS Spot 1 (a)

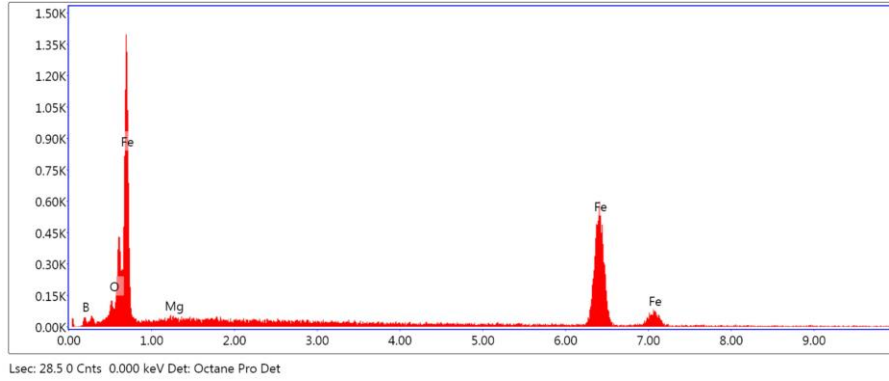


eZAF Smart Quant Results

Element	Weight %	Atomic %	Net Int.	Error %	Kratio	Z	R	A	F
B K	11.27	33.22	2.65	24.91	0.02	1.2	0.86	0.16	1
O K	6.54	13.03	55.10	9.70	0.04	1.21	0.9	0.49	1
MgK	9.24	12.12	84.66	10.41	0.04	1.12	0.94	0.39	1
FeK	72.95	41.63	227.98	4.00	0.69	0.92	1.02	1	1.03

Figure 7.20. EDS analysis results for <1 wt. % Mg-coated wire synthesized at 700°C for 1h. The locations of spots 1 (a) and 6 (b, on the next page) are shown in Figure 7.19.

EDS Spot 6 (b)



eZAF Smart Quant Results

Element	Weight (%)	Atomic (%)	Net Int.	Error (%)	Kratio	Z	R	A	F
B K	21.18	55.68	6.84	17.96	0.05	1.2	0.87	0.2	1
O K	2.96	5.26	25.80	11.56	0.02	1.21	0.91	0.45	1
MgK	0.69	0.81	7.04	29.49	0.00	1.11	0.94	0.38	1
FeK	75.17	38.26	266.47	3.82	0.71	0.92	1.03	1	1.03

Figure 7.20. (cont'd) EDS analysis results for <1wt. % Mg-coated wire synthesized at 700°C for 1h. The locations of spots 1 and 6 are shown in Figure 7.19.

Spot analysis was performed by using EDS to analyze a region around single spots in order to obtain a spectrum showing elements present in that region. The EDS results from the spots 1 and 6 in Fig. 7.19 are shown in Figures 7.20(a) and (b), respectively. Fig. 7.20(a) represents the EDS result for spot 1 which was selected from the top of the small grains located just below the upper layer of relatively larger grains. Atomic percentages of Mg, Fe, O and B and grain characteristics in the spot 1 region indicated that the bottom layer was formed by MgB₂ grains. Oxygen is related to MgO content of the superconductor. Fig. 7.20(b) represents the results from the spot 6 which was selected from the upper layer forming near the core/sheath interface region. When the atomic percentages of the elements were examined on the upper lateral surface near the sheath material, it was revealed that the top layer was dominated by the FeB and Fe₂B phases. The Mg-coating process was thought to increase the critical current density of the MgB₂ wire under the external magnetic field by contributing to the formation of small MgB₂ grain structures in the bottom layers close to the core/interface region.

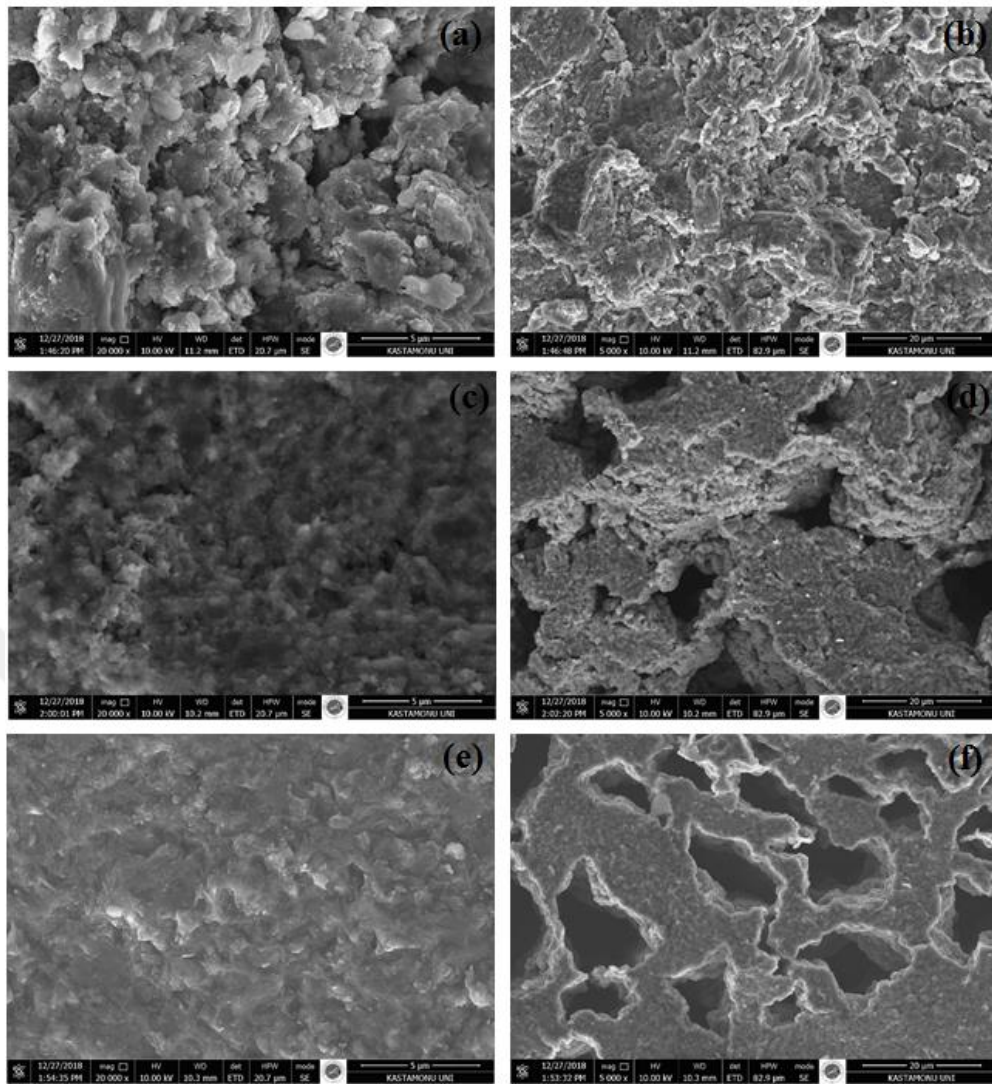


Figure 7.21. Micrographs for (a-b) the normal (stoichiometric) sample synthesized at 750°C for 1h, (c-d) <1wt. % Mg-coated sample synthesized at 700°C for 1h, and (e-f) 5wt. % excess-Mg sample synthesized at 700°C for 1h. Magnifications are 20000× at left column and 5000× at right column. These samples were produced by using PeIT method.

Figures 7.21(a) to (f) represent the SEM images of MgB₂ superconducting core microstructures of normal (stoichiometric), 5wt. % excess-Mg, and Mg-coated (<1wt. %) wire samples. These images were taken from the cross-sectional fracture surface of the samples at two different magnifications; (a), (c) and (e) at x20000 magnification and (b), (d) and (f) at X5000 magnification. It was found in Figs. 7.21(a) and 7.21(c) that Mg-coated and normal wires had almost the same sized MgB₂ grains but the grains of the normal sample had scattered orientations in different directions and more and larger voids accompanied with slightly loose appearance were observed in this sample. The grains with different directions and existence of small voids may explain the low A_F

values found for the normal sample in Table 7.2. Fig. 7.21(e) shows that 5 wt. % excess-Mg sample has a molten structure because it contains more melted Mg which is capable both to react with the B particles to form more MgB_2 and also to fill the gaps between the grains. On the other hand, large gaps resulting from the diffusion of excess amount of Mg during chemical reaction interrupted successive Mg/ MgB_2 occurrences as shown in Figure 7.21(f). These gaps were also observed in the Mg coated wire sample as shown in Figure 7.21(d), but they are smaller in size and number when compared with the 5wt. % excess Mg-containing sample.



8. CONCLUSIONS

The main purpose of this thesis is to find a way of improving the transport properties of MgB₂/Fe superconducting wires under low/medium magnetic fields without use of any chemical additions or barrier material. The Mg-coating method was proposed to achieve this goal because the positive effect of excess Mg on transport properties of MgB₂ was enhanced by external Mg diffusion and reduced porosity. On the other hand, coated magnesium along the inner surface of the Fe sheath was expected to reduce Fe₂B formations by inhibiting boron diffusion, but structural and morphological analysis results showed that the Fe₂B phase was still present.

Magnesium was coated on the inner surface of the iron tubes successfully according to the result of the elemental map analysis. The XRD patterns demonstrated that the Fe₂B formations existed between the core and sheath interface region for all samples, so that, the Mg coating method did not behave as a diffusion barrier. On the other hand, Mg coating method has been found to be a very effective method for improving the transport properties of MgB₂ superconducting wire. This improvement was first revealed when a comparison was made between normal wires and Mg-coated wires. J_{ce} exceeded 10^2A/cm^2 at 28K and under $B = 6.75\text{T}$ for Mg-coated wires. Same wires were also tested at liquid helium environment ($T = 4.2\text{K}$) and J_{ce} was found above 10^4A/cm^2 under moderate magnetic field of 5T. The $J_{ce} - B$ behavior of Mg-coated wire was further improved when the wires were fabricated by using the PeIT method and the same J_{ce} level of 10^2A/cm^2 was reached under $B = 7\text{T}$ at 28K. Our studies showed that even the samples having 5wt. % excess Mg addition did not reach this J_{ce} level. It was also revealed that there was a significant difference between n -values of normal and non-stoichiometric wires. Moreover, n -value was further improved for the Mg-coated wire and $n = 4.8$ was achieved at $T = 28\text{K}$ and $B = 7\text{T}$.

The temperature dependent resistivity measurements showed that superconducting wire samples containing excess amount of Mg had better and sharper superconducting phase transition in comparison to the normal samples. The effect of excessive magnesium on the resistivity and connectivity of the stripped wires were also analyzed as a function of synthesis conditions. It was revealed that the RRR was increasing with increasing amount of excessive Mg but A_F values are dependent on the

heat treatment conditions (see Table 7.2). The RRR and A_F values for Mg-coated samples were found to be almost independent of the differences in heat treatment conditions unlike the samples containing 1wt. % and 5wt. % excess-Mg.

In the Mg-coating method, the excess of Mg was provided by an external diffusion process into the Mg+2B powder. In this way, an extra porosity was inhibited due to the fact that excess Mg particles were not incorporated into the reaction through the powder. However, 5wt. % excess-Mg wire samples had large voids left by excess Mg particles during the reaction (see Figure 7.21(f)). The SEM results showed that Mg-coating method provided the formation of small MgB_2 grains with more grain boundaries in a region close to core/sheath interface and improved the pinning properties of MgB_2 wire under medium magnetic fields.

We suggest that Mg coating method can be preferable to obtain a reproducible, high performance, stable and cost-effective *in-situ* MgB_2/Fe wires. As a future work, this method of internal Mg-coating presented in this thesis, can be studied for the reduction of boron rich zones. In order to reduce the amount of un-reacted B particles, it was attempted to add Mg to IMD MgB_2 wires, but this resulted in the formation of a porous structure (Ye, 2014). It is necessary to avoid un-reacted B particles, to obtain small enough voids and to achieve lower MgO quantities at the same time.

9. REFERENCES

- Abrikosov AA (1957) "The magnetic properties of superconducting alloys", *Journal of Physics and Chemistry of Solids*, 2: 199-208.
- Akdoğan M, Yetis H, Gajda D, Karaboga F, Ülgen AT, Demirtürk E, Belenli I (2015) "Effect of the initial filling density on the critical current of in-situ Fe/MgB₂ wires", *Journal of Alloys and Compounds*, 649: 1007-1010.
- Akdoğan M, Yetiş H, Gajda D, Karaboğa F, Rogacki K, Morawski A, Belenli İ (2017) "Use of amorphous boron and amorphous nano boron powder mixture in fabrication of long in-situ MgB₂/Fe wires", *Journal of Alloys and Compounds*, 702: 399-403.
- Akimitsu J, Nagamatsu J, Nakagawa N, Muranaka T, Zenitani Y (2001) "Superconductivity at 39 K in magnesium diboride", *Nature*, 410: 63-64.
- An JM, and Pickett WE (2001) "Superconductivity of MgB₂: Covalent Bonds Driven Metallic", *Phys Rev Lett*, 86:4366-4374.
- Angst M, Puzniak R, Wisniewski A, Jun J, Kazakov SM, Karpinski J, Roos J, and Keller H (2002) "Temperature and Field Dependence of the Anisotropy of MgB₂", *Phys Rev Lett*, 88: 167004-4.
- Armstrong DR, and Perkins PG (1979) "Electronic band structure of magnesium diboride", *Journal of the Chemical Society, Faraday Transactions 2: Molecular and Chemical Physics*.
- Atomura N, Takahashi T, Amata H, Iwasaki T, Kyoung-woo S, Miyagi D, Tsuda M, Hamajima T, Shintomi T, Makida Y, Takao T, Munakata K, Kajiwara M (2012) "Conceptual design of MgB₂ coil for the 100 MJ SMES of advanced superconducting power conditioning system (ASPCS)", *Physics Procedia*, 27: 400-403.
- Bardeen J, Cooper LN and Schrieffer JR (1957) "Theory of Superconductivity", *Physical Review B*, 108: 1175-1204.
- Bud'ko SL, Lapertot G, Petrovic C, Cunningham CE, Anderson N and Canfield PC (2001) "Boron Isotope Effect in Superconducting MgB₂", *Phys Rev Lett*, 86: 1877-1880.
- Buzea C and Yamashita T (2001) "Review of the superconducting properties of MgB₂", *Supercond Sci Technol*, 14: 112-146.
- Cetner T, Morawski A, Adamczyk K, Rindfleisch M, Tomsic M, Zaleski A, Gajda D and Presz A (2012) "Improvement of critical properties of undoped, multifilamentary MgB₂ wires in Nb/Cu after annealing under high gas pressure", *High Pressure Research*, 32: 419-424.

- Cetner T, Morawski A, Gajda D, Häbller W, Rindfleisch M, Tomsic M, Zaleski A, Czujko T, Żuchowska E and Przysławski P (2015) “Hot isostatic pressing of multifilamentary MgB₂ wires in solid state media for large scale application”, *Supercond Sci Technol*, 28: 045009-6.
- Chauhan SR and Chaudhary S (2010) “On the Residual Resistivity Ratio in MgB₂ Superconductors”, *IEEE Trans on Appl Supercond*, 20: 26 – 32.
- Chen SK, Serquis A, Serrano G, Yates KA, Blamire MG, Guthrie D, Cooper J, Wang H, Margadonna S and MacManus-Driscoll JL (2008) “Structural and Superconducting Property Variations with Nominal Mg Non-Stoichiometry in Mg_xB₂ and Its Enhancement of Upper Critical Field”, *Advanced Functional Materials*, 18: 113-120.
- Choi HJ, Roundy D, Sun H, Cohen ML and Louie SG (2002) “First-principles calculation of the superconducting transition in MgB₂ within the anisotropic Eliashberg formalism”, *Phys Rev B*, 66: 020513-4.
- Collings EW, Sumption MD, Bhatia M, Susner MA and Bohnenstiehl SD (2008) “Prospects for improving the intrinsic and extrinsic properties of magnesium diboride superconducting strands”, *Supercond Sci Technol*, 21: 103001-14.
- Dou SX, Yeoh WK, Shcherbakova O, Wexler D, Li Y, Ren ZM, Munroe P, Chen SK, Tan KS, Glowacki BA and MacManus-Driscoll JL (2006) “Alignment of Carbon Nanotube Additives for Improved Performance of Magnesium Diboride Superconductors”, *Advanced Materials*, 18: 785-788.
- Flükiger R (2016) *MgB₂ Superconducting Wires Basics and Applications Vol.2* World Scientific Co. Pte. Ltd. Singapore.
- Flükiger R, Suo HL, Musolino N, Beneduce C, Toulemonde P, and Lezza P (2003) “Superconducting properties of MgB₂ tapes and wires”, *Physica C*, 385: 286–305.
- Gajda D, Morawski A, Zaleski A, Cetner T, Małecka M, Presz A, Rindfleisch M, Tomsic M, Thong CJ and Surdacki P (2013) “Comparison of critical current density in SiC-doped in situ MgB₂ coils and straight wire samples processed by HIP”, *Supercond Sci Technol*, 26: 115002-8.
- Gajda D, Morawski A, Zaleski AJ, Cetner T, Häbllere W, Nenkov K, Małecka M, Rindfleisch MA, Tomsic M (2018) “Significant enhancement of the critical current of MgB₂ wires through a reduction of the diameter using HIP method”, *Scripta Materialia*, 143: 77-80.
- Gao Z, Wang D, Zhang X, Ma Y, Awaji S, Nishijima G, Watanabe K, and Flukiger R (2010) “Simultaneous introduction of scattering and pinning in organic rare-earth salt doped MgB₂ tapes”, *Supercond Sci Technol*, 23: 045024-4.

- Garland JW (1963) “Isotope Effect in Superconductivity”, *Phys Rev Lett*, 11: 114-119.
- Ghorbani SR, Farshidnia G, Wang XL and Dou SX (2014) “Flux pinning mechanism in SiC and nano-C doped MgB₂: evidence for transformation from δT_c to δl pinning”, *Supercond Sci Technol*, 27: 125003-7.
- Gi-Dong N, Hae-Jin S, Byeong-Soo G, Park M and In-Keun Y (2018) “Design and Comparative Analysis of MgB₂ and YBCO Wire Base Superconducting Wind Power Generators”, *IEEE Trans on App Supercond*, 28: 5205605-5205609.
- Giunchi G, Ceresara S, Ripamonti G, Di Zenobio A, Rossi S, Chiarelli S, Spadoni M, Wesche R and Bruzzone PL (2003) “High performance new MgB₂ superconducting hollow wires”, *Supercond Sci and Technol*, 16: 285-291.
- Glowacki BA, Majoros M, Vickers M, Evetts JE, Shi Y, and McDougall I (2001) “Superconductivity of powder-in-tube MgB₂ wires”, *Supercond Sci and Technol*, 14: 193-199.
- Grivel JC, Andersen NH, Pinholt R, Kovác P, Husek I, Hässler W, Herrmann M, Perner O, Rodig C and Homeyer J (2006) “In-situ studies of Fe₂B phase formation in MgB₂ wires and tapes by means of high-energy x-ray diffraction”, *Journal of Physics: Conference Series*, 43:123-126.
- Hascicek YS, Akin Y, Baldwin TW, Rindfleisch MM, Yue J, Sumption MD, and Tomsic M (2009) “A MgB₂ 12.5 kVA superconductor transformer”, *Supercond Sci Technol*, 22: 065002-7.
- Hata S, Yoshidome T, Sosiati H, Tomokiyo Y, Kuwano N, Matsumoto A, Kitaguchi H and Kumakura H (2006) “Microstructures of MgB₂/Fe tapes fabricated by an in situ powder-in-tube method using MgH₂ as a precursor powder”, *Supercond Sci and Technol* 19: 161–168.
- Hinks DG, Claus H and Jorgensen JD (2001) “The complex nature of superconductivity in MgB₂ as revealed by the reduced total isotope effect”, *Nature*, 411: 457-460.
- Hossain MSA, Motaman A, Barua S, Patel D, Mustapic M, Kim JH, Maeda M, Rindfleisch M, Tomsic M and Cicek O (2014) “The roles of CHPD: superior critical current density and n-value obtained in binary in situ MgB₂ cables”, *Supercond Sci and Technol*, 27: 095016-7.
- Hur JM, Togano K, Matsumoto A, Kumakura H, Wada H and Kimura K (2008) “Fabrication of high-performance MgB₂ wires by an internal Mg diffusion process”, *Supercond Sci and Technol*, 21: 032001-4.

- Jiang CH and Kumakura H (2007) "Stoichiometry dependence of the critical current density in pure and nano-SiC doped MgB₂/Fe tapes", *Physica C*, 451: 71–76.
- Jiang CH, Nakane T and Kumakura H (2005) "Superior high-field current density in slightly Mg-deficient MgB₂ tape", *Appl Phys Lett*, 87: 252505-3.
- Jiang J, Senkowicz BJ, Larbalestier DC and Hellstrom EE (2006) "Influence of boron powder purification on the connectivity of bulk MgB₂", *Supercond Sci and Technol*, 19: L33-L36.
- Jie H, Qiu W, Billah M, Mustapic M, Patel D, Ma Z, Gajda D, Morawski A, Cetner T, Shahabuddin M, Yanmaz E, Rindfleisch M, Kim JH, Hossain MSA (2017) "Superior transport J_c obtained in in-situ MgB₂ wires by tailoring the starting materials and using a combined cold high pressure densification and hot isostatic pressure treatment", *Scripta Materialia*, 129: 19-83.
- Karaboğa F, Avcı D, Yetis H, Akdoğan M, Gajda D, Belenli I (2017) "Improvement of *in-situ* Fe/MgB₂ monofilamentary wires by internal Mg-coating process", *Journal of Alloys and Compounds*, 727: 20-26.
- Karaboğa F, Yetiş H, Akdoğan M, Belenli İ (2018) "Monofilamentary in Situ Fe/MgB₂ Superconducting Wires Fabricated by Pellet-in-Tube Method", *J Superconductivity and Novel Magnetism*, 31: 1359-1367.
- Kim JH, Dou SX, Hossain MSA, Xu X, Wang JL, Shi DQ, Nakane T, and Kumakura H (2007) "Systematic study of a MgB₂ + C₄H₆O₅ superconductor prepared by the chemical solution route", *Supercond Sci Technol*, 20: 715–719.
- Kim JH, Heo Y, Matsumoto A, Kumakura H, Rindfleisch M, Tomsic M and Dou SX (2010) "Comparative study of mono- and multi-filament MgB₂ wires with different boron powders and malic acid addition", *Superconductor Science and Technology*, 23:075014-7.
- Kim JH, Oh S, Heo Y, Hata S, Kumakura H, Matsumoto A, Mitsuhashi M, Choi S, Shimada Y, Maeda M, MacManus-Driscoll JL and Dou SX (2012) "Microscopic role of carbon on MgB₂ wire for critical current density comparable to NbTi", *NPG Asia Materials*, 4:1-7.
- Kim JH, Yeoh WK, Qin MJ, Xu X and Dou SX (2006) "The doping effect of multiwall carbon nanotube on MgB₂/Fe superconductor wire", *J Appl Phys* 100: 013908-6.
- Klie RF, Idrobo JC, and Browning ND (2001) "Direct observation of nanometer-scale Mg- and B-oxide phases at grain boundaries in MgB₂", *Appl Phys Lett*, 79: 1837-1839.

- Kortus J, Mazin II, Belashchenko KD, Antropov VP and Boyer LL (2001) "Superconductivity of Metallic Boron in MgB_2 ", *Phys Rev Lett*, 86: 4656-4664.
- Koshelev AE and Golubov AA (2004) "Why Magnesium Diboride Is Not Described by Anisotropic Ginzburg-Landau Theory", *Phys Rev Lett*, 92: 107008-4.
- Kováč P, Hušek I, Melišek T, Štrbík V and Kulich M (2006) " MgB_2 composite wires with Fe, Nb and Ta sheaths", *Supercond Sci and Technol*, 19: 600-605.
- Li GZ, Sumption MD, Susner MA, Yang Y, Reddy KM, Rindfleisch MA, Tomsic MJ, Thong CJ, and Collings EW (2012) "The critical current density of advanced internal-Mg-diffusion-processed MgB_2 wires", *Supercond Sci and Technol*, 25: 115023-8.
- Li WX, Li Y, Chen RH, Zeng R, Lu L, Zhang Y, Tomsic M, Rindfleisch M and Dou SX (2009) "Increased Superconductivity for CNT Doped MgB_2 Sintered in 5T Pulsed Magnetic Field", *IEEE Transc on App Supercond*, 19: 2752-2755.
- Maeda M, Hossain MSA, Motaman A, Kim JH, Kario A, Rindfleisch M, Tomsic M, and Dou SX (2013) "Synergetic Combination of LIMD With CHPD for the Production of Economical and High Performance MgB_2 Wires", *IEEE Trans on App Supercond*, 23: 6200704-4.
- Marauchkine A (2004) *Room-Temperature Superconductivity*, Cambridge International Science Publishing, Cambridge.
- Martínez E, Mikheenko P, Martínez-López M, Millán A, Bevan A, and Abell J S (2007) "Flux pinning force in bulk MgB_2 with variable grain size", *Phys. Rev B*, 75: 134515-8.
- Matsushita T, Kiuchi M, Yamamoto A, Shimoyama J, Kishio K (2008) "Critical current density and flux pinning in superconducting MgB_2 ", *Physica C: Superconductivity*, 468: 1833-1835.
- Matsushita T, Kiuchi M, Yamamoto A, Shimoyama Jun-ichi, and Kishio K (2007) "Essential factors for the critical current density in superconducting MgB_2 : connectivity and flux pinning by grain boundaries", *Supercond Sci and Technol*, 21: 015008-7.
- Maxwell E (1950) "Isotope Effect in the Superconductivity of Mercury", *Phys Rev*, 78: 477.
- Mikheenko P, Martínez E, Bevan A, Abell JS and MacManus-Driscoll JL (2007) "Grain boundaries and pinning in bulk MgB_2 ", *Superconductor Sci and Technol*, 20: S264-S270.

- Moshchalkov V, Menghini M, Nishio T, Chen QH, Silhanek AV, Dao VH, Chibotaru LF, Zhigadlo ND and Karpinsk J (2009) “Type-1.5 Superconductivity”, *Phys Rev Lett*, 102: 117001-4.
- Motaman A, Barua S, Patel D, Maeda M, Cheong K, Kim JH, Dou SX, Hossain MSA (2014) “Power-Law Relationship Between Critical Current Density, Microstructure, and the n-Value in MgB₂ Superconductor Wires”, *J Superconductivity and Novel Magnetism*, 27: 1643-1645.
- Motaman A, Hossain MSA, Xu X, See KW, Chung KC and Dou SX (2013) “A comprehensive study of the pinning mechanisms of MgB₂ wires treated with malic acid and their relationships with lattice defects”, *Supercond Sci Technol*, 26: 085013-6.
- OF de Lima and Cardoso CA (2003) “Anisotropy in MgB₂”, *Brazilian Journal of Physics*, 33: 709-712.
- Park DK, Ling J, Rindfleisch M, Voccio J, Hahn S, Bascuñán J, Tomsic M and Iwasa Y (2012) “MgB₂ for MRI Magnets: Test Coils and Superconducting Joints Results”, *IEEE Trans on App Supercond*, 22: 4400305-5.
- Prikhna TA, Romaka VV, Shapovalov AP, Eisterer M, Sokolovsky V, Weber HW, Grechnev GE, Boutko VG, Gusev AA, Kozyrev AV, Goldacker W, Moshchil VE, Sverdun VB, Habisreuther T, Schmidt C, Kovylaev VV, Shaternik VE, Karpets MV and Shaternik AV (2017) “Structure and Properties of MgB₂ Bulks, Thin Films, and Wires”, *IEEE Trans on App Supercond*, 27: 4.
- Ravindran P, Vajeeston P, Vidya R, Kjekshus A and Fjellvåg H (2001) “Detailed electronic structure studies on superconducting MgB₂ and related compounds”, *Phys Rev B*, 64: 224509-14.
- Reynolds CA, Serin B, Wright WH and Nesbitt LB (1950) “Superconductivity of Isotopes of Mercury”, *Phys Rev*, 78: 487.
- Rowell JM (2003) “The widely variable resistivity of MgB₂ samples”, *Supercond Sci Technol*, 16: 17-27.
- Schlachter SI, Frank A, Ringsdorf B, Orschulko H, Obst B, Liu B and Goldacker W (2006) “Suitability of sheath materials for MgB₂ powder-in-tube superconductors”, *Physica C: Superconductivity and its Applications*, 445-448: 777-783.
- Schmidt VV (1997) *The Physics of Superconductors*, Springer-Verlag Berlin Heidelberg, Berlin.
- Seidel P (2015) *Applied Superconductivity: Handbook on Devices and applications*, Markono Print Media Pte. Ltd., Singapore.

- Serquis A, Civale L, Hammon DL, Liao XZ, Coulter JY, Zhu YT, Jaime M, Peterson DE and Mueller FM (2003) “Hot isostatic pressing of powder in tube MgB₂ wires”, *Appl Phys Lett*, 82: 2847-2849.
- Sheahen TP (2002) *Introduction to High Temperature Superconductivity*, Western Technology Incorporated, Maryland.
- Susner MA, Sumption MD, Bhatia M, Peng X, Tomsic MJ, Rindfleisch MA and Collings EW (2007) “Influence of Mg/B ratio and SiC doping on microstructure and high field transport J_c in MgB₂ strands”, *Physica C* 456: 180–187.
- Susner MA, Sumption MD, Rindfleisch MA and Collings EW (2013) “Critical current densities of doped MgB₂ strands in low and high applied field ranges: The $J_c(B)$ crossover effect”, *Physica C*, 490: 20–25.
- Tomsic M, Rindfleisch M, Yuea J, McFaddena K, Doll D, Phillipsa J, Sumption MD, Bhatia M, Bohnenstiehl S and Collings EW (2007) “Development of magnesium diboride (MgB₂) wires and magnets using in situ strand fabrication method”, *Physica C*, 456: 203-208.
- Wan X, Dong J, Weng H and Xing DY (2001) “Band structure of MgB₂ with different lattice constants”, *Phys Rev B* 65: 012502-4.
- Wang D, Ma Y, Yao C, Xu D, Zhang X, and Awaji S (2017) “Transport properties of multifilament MgB₂ long wires and coils prepared by an internal Mg diffusion process”, *Supercond Sci and Technol*, 30: 6.
- Xiao H, Peng W, Song WH, Ma RC, Zhang L, Du JJ and Sun YP (2003) “Influence of Mg deficiency on the properties of MgB₂”, *Physica C*, 386: 648–652.
- Xu M, Kitazawa H, Takano Y, Ye J, Nishida K, Abe H., Matsushita A, Tsujii N and Kido G, “Anisotropy of superconductivity from MgB₂ single crystals”, *Appl Phys Lett*, 79: 2779-2781.
- Yamamoto A, Shimoyama J, Kishio K and Matsushita T (2007) “Limiting factors of normal-state conductivity in superconducting MgB₂: an application of mean-field theory for a site percolation problem”, *Supercond Sci Technol*, 20: 658-666.
- Yang Y (2016) “Influence of Chemical Doping on Microstructures and Superconducting Properties of MgB₂ Wires and Bulk Samples”, Doctor of Philosophy, Ohio State University, Material Science and Engineering.
- Ye L, Majoros M, Campbell AM, Coombs T, Astill D, Harrison S, Husband M, Rindfleisch M and Tomsic M (2007) “Experimental studies of the quench behaviour of MgB₂ superconducting wires for fault current limiter applications”, *Supercond Sci Technol*, 20: 621-628.

- Ye SJ, Matsumoto A, Togano K, Zhang YC, Ohmura T and Kumakura H (2014) “Fabrication of MgB₂ superconducting wires with a hybrid method combining internal-Mg-diffusion and powder-in-tube processes”, *Supercond Sci and Technol*, 27: 055017-6.
- Yetis H, Karaboga F, Avcı D, Akdogan M and Belenli I (2019) “Role of novel Mg-coating method on transport properties of MgB₂/Fe wires”, *Physica C*, 562: 13-19.
- Zehetmayer M (2013) “A review of two-band superconductivity: materials and effects on the thermodynamic and reversible mixed-state properties”, *Supercond Sci Technol*, 26: 043001-6.
- Zeng R, Lu L, Wang JL, Horvat J, Li WX, Shi DQ, Dou SX, Tomsic M and Rindfleisch M (2007) “Significant improvement in the critical current density of in situ MgB₂ by excess Mg addition”, *Supercond Sci Technol*, 20: L43-L47.
- Zhang H, Zhao Y and Zhang Y (2015) “The Effects of Excess Mg Addition on the Superconductivity of MgB₂”, *J Supercond Nov Magn*, 28: 2711–2714.

10. CURRICULUM VITAE

Name SURNAME : Dođan Avcı

Place and Date of Birth : Tekirdađ, 02.09.1991

Universities

Bachelor's Degree : Bolu Abant İzzet Baysal University

E-mail : davci.0209@gmail.com

Address : Bahçelievler Mahallesi, Yümnüođlu Sokak, Eren Apartmanı, No: 8 Daire: 8.

Projects

- TÜBİTAK 216M300, “Sfcl Özelliikli Dađıtım Transformatörü (Sdtr)”, 01.07.2017 01.07.2020.
- AİBÜ-BAP 2017.03.02.1193 “MgB₂ Süperiletken Tellerin 3 Eksenli Silindirik Hadde ile Sođuk Sıkılaştırılması”, 30.05.2017 - 30.05.2018.

Conferences

- A.T. Ulgen, I. Belenli, F. Karaboga, D. Avcı, B. Albayrak “ Effects of Au diffusion on magnetic properties of Ex-situ and In-situ MgB₂ Superconductors ” INTERNATIONAL CONFERENCE ON CONDENSED MATTER AND MATERIAL SCIENCES 2017 | 11-15 October, Adana (Poster)

List of Publications

- F. Karaboga, I. Belenli, H. Yetis, M. Akdogan, D. Avcı, D. Gajda (2017) “Improvement of in-situ Fe/MgB₂ monofilamentary wires by internal Mg-coating process” JALCOM, 727: 20-26.
- Yetiş H., Karabođa F., Avcı D., Akdođan M., and Belenli İ. (2019) “Role of novel Mg-coating method on transport properties of MgB₂/Fe wires”, Physica C: Superconductivity and its Applications, 562: 13-19.